eLife

Reviewed Preprint
v1 • May 12, 2026
Not revised

For correspondence:
tampe@em.uni-frankfurt.de

Competing interests: No competing interests declared

Funding: See page 21

Reviewing editor: Camilo Perez, University of Georgia, United States

ATP-driven conformational dynamics reveal hidden intermediates in a heterodimeric ABC transporter

Matija Pečak, Christoph Nocker, Robert Tampé

Institute of Biochemistry, Biocenter, Goethe University Frankfurt, Frankfurt am Main, Germany

eLife Assessment

The study presents **important** findings revealing previously unresolved conformational dynamics of the heterodimeric type IV ABC transporter TmrAB using single-molecule FRET. The evidence presented is **solid**, integrating careful experimental design with computational approaches to uncover states that are typically masked and difficult to detect. The work will be of interest to scientists studying the molecular mechanisms of primary active transport processes.

https://doi.org/10.7554/eLife.110967.1.sa2

Abstract

ATP-binding cassette (ABC) transporters are essential molecular machines whose conformational dynamics have largely been inferred from ensemble-averaged measurements. Resolving dynamic heterogeneity and transient intermediates, however, requires single-molecule approaches. Here, we use single-molecule Förster resonance energy transfer (smFRET) to directly monitor conformational changes of the heterodimeric type IV ABC transporter TmrAB, a functional homolog of the human antigen transporter TAP. Fluorophores positioned at the nucleotide-binding domains and the periplasmic gate were validated by accessible-volume simulations, fluorescence lifetimes, and ensemble FRET, demonstrating that these reporters reliably track conformational transitions. Single-molecule analysis distinguishes ATP-free and ATP-bound states and reveals ATP-dependent population shifts from nucleotide-free to physiological ATP concentrations. Probing conformational dwell-times further uncovers an unexpectedly long ATP-bound dwell time of ~300 ms. Using complementary stabilization strategies–including a slow-turnover variant, Mg^{2+} depletion, or substrate trans-inhibition–we resolve a previously hidden outward-facing open state that rapidly interconverts with occluded intermediates under turnover conditions. These results provide the first single-molecule characterization of TmrAB and establish a general framework for dissecting ATP-coupled conformational dynamics in heterodimeric ABC transporters.

Introduction

ATP-binding cassette (ABC) transporters constitute the largest family of primary active membrane transport systems, conserved across all domains of life[1–3]. Despite considerable structural diversity, all ABC transporters share a modular architecture comprising two conserved nucleotide-binding domains (NBDs)–the defining hallmark of the family–and two transmembrane domains (TMDs) that form the substrate translocation pathway[3,4]. Based on their transmembrane-domain architecture, ABC transporters are classified into seven types that encompass importers, exporters, extractors, and mechanotransmitters[5]. Substrate translocation is driven by large conformational changes that are chemo-mechanically coupled to ATP binding, hydrolysis, and phosphate/ADP release[2,3]. ABC transporters play central roles in cellular homeostasis, nutrient uptake, waste removal, and toxin defense. Their dysfunction and misregulation are linked to numerous diseases and drug resistance[6].

The heterodimeric type IV ABC transporter TmrAB from *Thermus thermophilus* has emerged as a powerful model system due to its exceptional thermal stability and functional homology to the transporter associated with antigen processing (TAP1/2), a key component of adaptive immunity[7–9]. Notably, TmrAB shares overlapping peptide specificity with TAP and can restore antigen presentation in TAP-deficient human cells[10]. Its inherent asymmetry, with one catalytically active (canonical) and one inactive (noncanonical) nucleotide-binding site (NBS), provides a unique opportunity to investigate functional specialization and asymmetry in ABC transport mechanisms.

Extensive structural studies, particularly using cryogenic electron microscopy (cryo-EM), have delineated the conformational landscape of TmrAB and yielded a detailed model of its translocation cycle[11,12]. In this model, TmrAB fluctuates between inward-facing wide and narrow conformations (IF^{wide} and IF^{narrow}), characterized by a sealed periplasmic gate (PG) and well-separated NBDs, thereby permitting substrate access to the central binding cavity. ATP binding to both NBDs induces NBD dimerization and drives the transition into the outward-facing states, including an OF open (OF^{open}) conformation with an open PG that enables substrate release into the periplasm, as well as an OF occluded ($OF^{occluded}$) state characterized by a sealed PG and dimerized NBDs. Subsequent ATP hydrolysis and phosphate release lead to asymmetric unlocked return states (UR^{asym} and UR^{asym}*), before the transporter returns to the IF conformation. These UR sates feature as sealed PG, a partially open ADP-bound canonical NBS, and a tightly ATP-occluded noncanonical NBS[11].

Single-turnover experiments established that ATP binding, rather than hydrolysis, drives the IF-to-OF transition, while phosphate release precedes the OF-to-IF switch[12,13]. Complementary ensemble approaches, including pulsed electron–electron double resonance (PELDOR/DEER) spectroscopy, have further characterized ATP-dependent conformational changes[14,15]. However, ensemble averaging inherently masks molecular heterogeneity, obscures inactive or misfolded subpopulations, and limits access to kinetic information.

Single-molecule techniques overcome these limitations by resolving conformational dynamics at the level of individual molecules[16,17]. In particular, single-molecule Förster resonance energy transfer (smFRET) enables real-time monitoring of protein conformational changes with nanometer precision[18–21]. Applied to ABC transporters, smFRET provides a unique opportunity to dissect transport cycles, resolve transient intermediates, and extract kinetic and mechanistic insights that remain inaccessible to ensemble-based measurement approaches[22–24].

Here, we apply total internal reflection fluorescence (TIRF) microscopy combined with alternating laser excitation (ALEX)-based smFRET to detergent-solubilized heterodimeric ABC transporter TmrAB, providing the first single-molecule characterization of this system. By strategically positioning fluorophore pairs, we directly monitor ATP-dependent NBD dimerization and periplasmic gate (PG) opening, quantify conformational state occupancies across ATP concentrations ranging from nucleotide-free to physiological levels (3 mM), and uncover conformational dynamics previously masked by ensemble averaging. Using three orthogonal trapping strategies–(i) a slow-turnover catalytic mutant[11,12], (ii) Mg^{2+} depletion[14,25], and (iii) substrate trans-inhibition[26,27]–we resolved a previously hidden outward-facing open (OF^{open}) state that rapidly exchanges with the outward-facing occluded ($OF^{occluded}$) state. Distance measurements derived from smFRET closely matched predictions from accessible-volume (AV) simulations, cryo-EM structures, and PELDOR/DEER spectroscopy, confirming that detergent-solubilized TmrAB retains a native-like conformational landscape. Together, these results provide the first single-molecule quantification of conformational state occupancies for a heterodimeric type IV ABC transporter and establish TmrAB as a versatile model for single-molecule studies of ABC transport systems.

Results

Design of FRET-labeled TmrAB variants to probe conformational dynamics

To monitor conformational changes in distinct regions of TmrAB, we engineered FRET variants targeting the nucleotide-binding domains (NBDs) and the periplasmic gate (PG). The NBDs undergo ATP-dependent dimerization followed by post-hydrolysis dissociation, whereas the PG opening and closing controls substrate release into the periplasm[2,3,11]. Probing both regions provides complementary readouts of cytosolic and periplasmic coupling during the transport cycle.

Labeling positions were selected based on prior PELDOR/DEER studies[15]. The NBD reporter variant (TmrA^{C416}B^{L458C}, referred to as TmrAB^{NBD}) monitors conformational changes at the noncanonical nucleotide-binding site (NBS), while the PG reporter (TmrA$^{C416A,\ T61C}$B^{R56C}, hereafter TmrAB^{PG}) tracks PG opening. In TmrAB^{NBD}, the native single cysteine (C416) was retained for labeling, whereas in TmrAB^{PG} it was substituted by alanine to prevent off-target labeling. Selecting the noncanonical rather than the canonical NBS prevents distinguishing outward-facing occluded (OF^{occluded}) from asymmetric unlocked return states (UR^{asym} and UR^{asym*})[11], but reduces the number of resolvable FRET states and thereby simplifies data interpretation.

Both variants were labeled with photostable fluorophores, LD555 (donor) and LD655 (acceptor), containing a 1,3,5,7-cyclooctatetraene moiety to suppress photobleaching and blinking[28,29]. Accessible-volume (AV) simulations[30] performed on nine cryo-EM structures[11] confirmed that donor-acceptor distances (R_{DA}) and simulated FRET efficiencies (E_{sim}) fall within the FRET-sensitive range (Fig. 1). For TmrAB^{NBD}, E_{sim} ranged from 0.62 ± 0.02 (57.9 ± 0.7 Å, NBDs separated) to 0.84 ± 0.01 (45.2 ± 0.4 Å, NBDs dimerized). For TmrAB^{PG}, E_{sim} shifted from 0.96 ± 0.02 (30.6 ± 0.4 Å, PG closed) to 0.69 ± 0.03 (53.8 ± 2.0 Å, PG open). These transitions correspond to ΔE_{sim} values of 0.22 and 0.27 and ΔR_{DA} of 12.7 Å and 23.2 Å, for TmrAB^{NBD} and TmrAB^{PG}, respectively, predicting robust and experimentally resolvable FRET changes.

Additionally, we employed a slow-turnover TmrAB variant that reports on PG opening (TmrA$^{C416A,\ E523Q,\ T61C}$B^{R56C}, hereafter TmrAB^{PG_EQ}). Substituting the catalytic glutamate with glutamine removed the carboxylate required to activate water for nucleophilic attack on ATP, thus drastically reducing the rate of ATP hydrolysis. This mutation slows down the catalytic turnover (~1000-fold) to a half-life of approximately 25 min at 45 °C[11,12,14,25], enabling stabilization of ATP-bound outward-facing conformations.

TmrAB variants are suitable for FRET studies

TmrAB variants were expressed in *E. coli* and purified using immobilized metal-affinity chromatography. SDS-PAGE and size-exclusion chromatography (SEC) confirmed high sample purity and monodispersity (Fig. 1–Fig. S1a,b). ATPase assays of TmrAB^{wt} verified that enzymatic activity was fully retained after purification, yielding a Michaelis-Menten constant (K_m) of 0.97 ± 0.28 mM and catalytic ATP turnover rate (k_{cat}) of 2.57 ± 0.38 s^{-1} at 40 °C (Fig. 1–Fig. S1c).

Cysteine-maleimide labeling of detergent-solubilized TmrAB variants achieved site-specific labeling efficiencies exceeding 90% (Fig. 1–Fig. S1d–f). Fluorescence lifetime (τ) analysis of conjugated fluorophores confirmed that their photophysical properties were preserved and that they retained sufficient rotational freedom for reliable FRET measurements. τ histograms of both conjugated and free fluorophores were fitted with a biexponential decay model, from which amplitude-weighted average lifetimes were calculated. For TmrAB^{NBD}, average τ values were 0.93 ± 0.02 ns (LD555) and 1.52 ± 0.01 ns (LD655), while TmrAB^{PG} exhibited average τ values of 0.95 ± 0.02 ns (LD555) and 1.65 ± 0.01 ns (LD655) (Fig. 1–Fig. S2a). By comparison, free dyes in buffer displayed lifetimes of 1.11 ± 0.02 ns (LD555) and 1.29 ±0.01 ns (LD655). Because the fluorescence lifetimes of both, the conjugated dyes and the free dyes, remain on the ~1 ns timescale, we conclude that the fluorophores remain photophysically active and are not affected by protein-induced quenching[17,31]. Moreover, the measured lifetimes on the nanosecond timescale are only

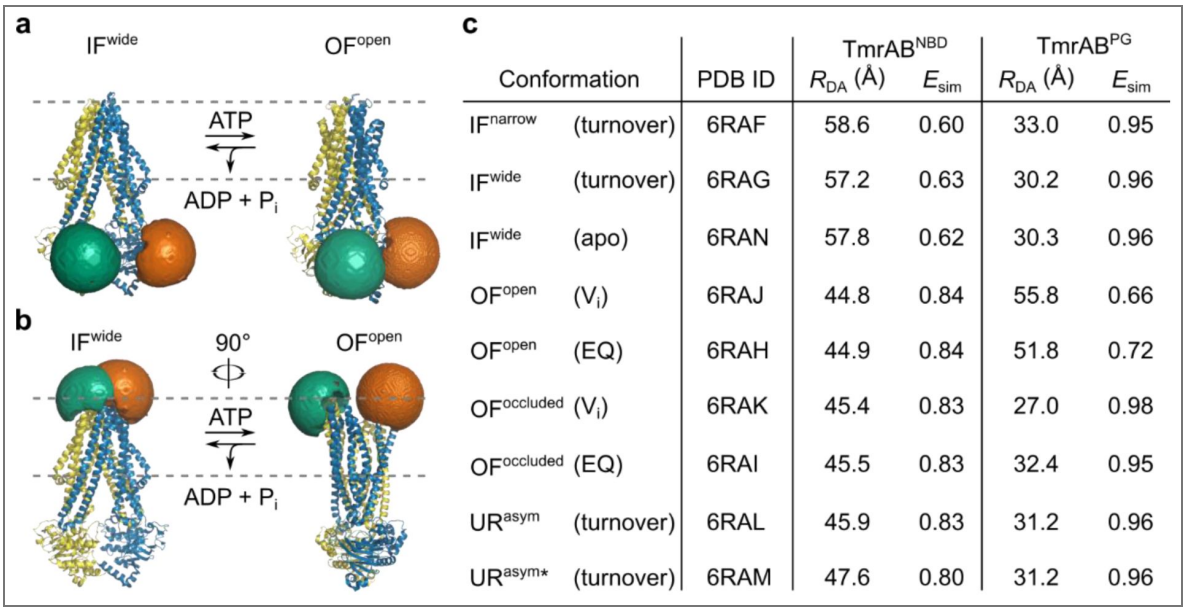

c

Conformation		PDB ID	TmrAB^{NBD} R_{DA} (Å)	TmrAB^{NBD} E_{sim}	TmrAB^{PG} R_{DA} (Å)	TmrAB^{PG} E_{sim}
IF^{narrow}	(turnover)	6RAF	58.6	0.60	33.0	0.95
IF^{wide}	(turnover)	6RAG	57.2	0.63	30.2	0.96
IF^{wide}	(apo)	6RAN	57.8	0.62	30.3	0.96
OF^{open}	(V_i)	6RAJ	44.8	0.84	55.8	0.66
OF^{open}	(EQ)	6RAH	44.9	0.84	51.8	0.72
OF^{occluded}	(V_i)	6RAK	45.4	0.83	27.0	0.98
OF^{occluded}	(EQ)	6RAI	45.5	0.83	32.4	0.95
UR^{asym}	(turnover)	6RAL	45.9	0.83	31.2	0.96
UR^{asym*}	(turnover)	6RAM	47.6	0.80	31.2	0.96

Figure 1. Accessible-volume (AV) simulations of LD fluorophores on TmrAB variants.

AV simulations were performed for LD555 (donor) and LD655 (acceptor) fluorophores attached to the selected TmrAB labeling sites to assess whether donor-acceptor distances are suitable for smFRET measurements[30]. **a**, TmrAB^{NBD} (TmrA^{C416}B^{L458C}) and **b**, TmrAB^{PG} (TmrA$^{C416A,\ T61C}$B^{R56C}) in the inward-facing wide (IF^{wide}; PDB: 6RAN, left) and outward-facing open (OF^{open}; PDB: 6RAH, right) conformations. Approximate membrane position is indicated by the dashed grey line. For all simulations, TmrA is shown in blue with LD655 (orange) and TmrB in yellow with LD555 (green). **c**, AV simulations confirmed that donor-acceptor distances (R_{DA}) remain within the FRET-sensitive range in both conformations, predicting measurable shifts in simulated FRET efficiencies (E_{sim}). Cryo-EM structures of TmrAB reconstituted in lipid nanodiscs[11] were used as templates. Structures were determined either in apo state (apo) or in presence of 3 mM ATP (turnover). Outward-facing open (OF^{open}) and outward-facing occluded (OF^{occluded}) structures were obtained via orthovanadate trapping (V_i) or by using the slow-turnover catalytic mutant TmrA^{E523Q}B (EQ).

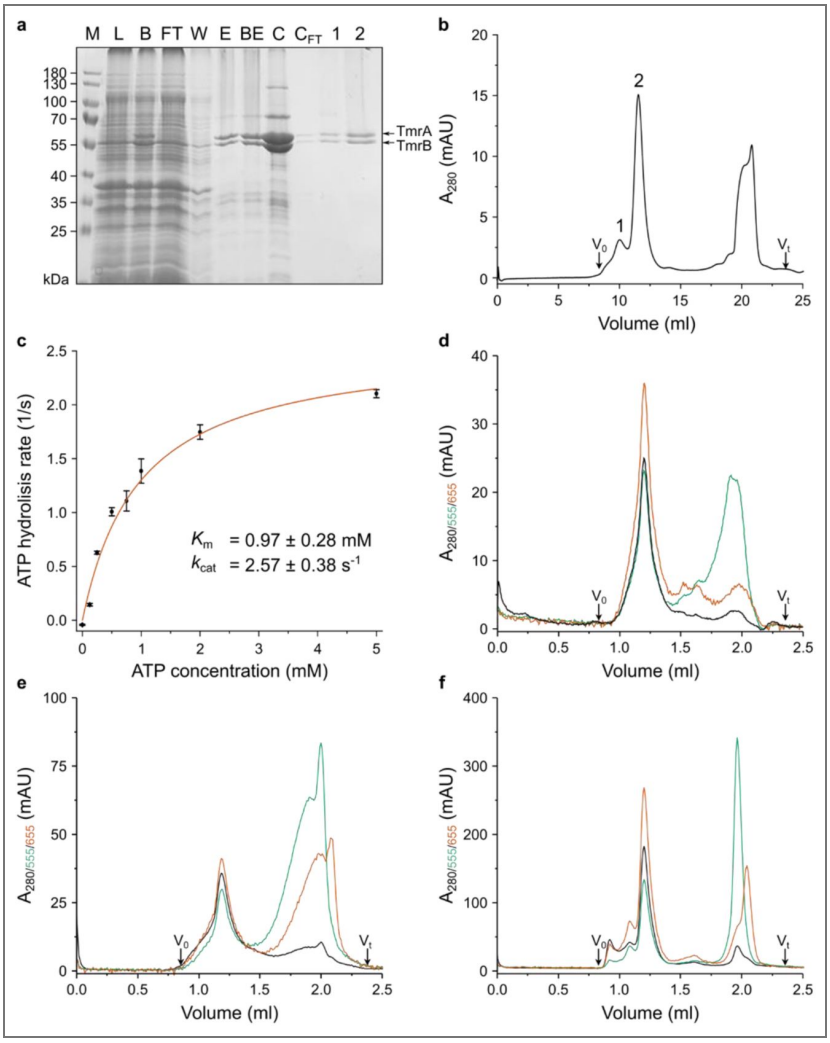

Figure 1 Figure supplement 1. Quality of TmrAB purification and fluorophore labeling.

a, SDS-PAGE analysis (10%, reducing conditions, Coomassie staining) of successive purification steps: M, molecular weight marker; L, cell lysate; B, Ni-NTA beads after incubation with lysate; FT, flow-through; W, wash; E, eluted TmrAB; BE, TmrAB after buffer exchange; C, concentrated TmrAB; CFT, concentrator flow-through; 1 and 2, first and second peaks eluted from size-exclusion chromatography (SEC). Only the second peak was used for subsequent FRET experiments. **b**, SEC (Superdex 200 increase 10/300 GL) confirming monodispersity of labeled TmrAB and efficient removal of free fluorophores. Representative chromatogram is shown for $TmrAB^{PG}$. **c**, ATP hydrolysis activity of purified wild-type TmrAB (60 nM $TmrAB^{wt}$) measured at 40 °C for 7 min. Released inorganic phosphate (P_i) was quantified using the Malachite Green assay. Data were fitted to a Michaelis-Menten model, yielding K_m = 0.97 ± 0.28 mM and k_{cat} = 2.57 ± 0.38 s^{-1}. **d**–**f**, Analytical SEC (Superdex 200 increase 3.2/300) used to determine fluorophore labeling efficiencies for each variant: (**d**) $TmrAB^{NBD}$, LD555: ~55%, LD655: ~53%; (**e**) $TmrAB^{PG}$, LD555: ~43%, LD655: ~52%; and (**f**) $TmrAB^{PG\_EQ}$, LD555: ~42%, LD655: ~52%.

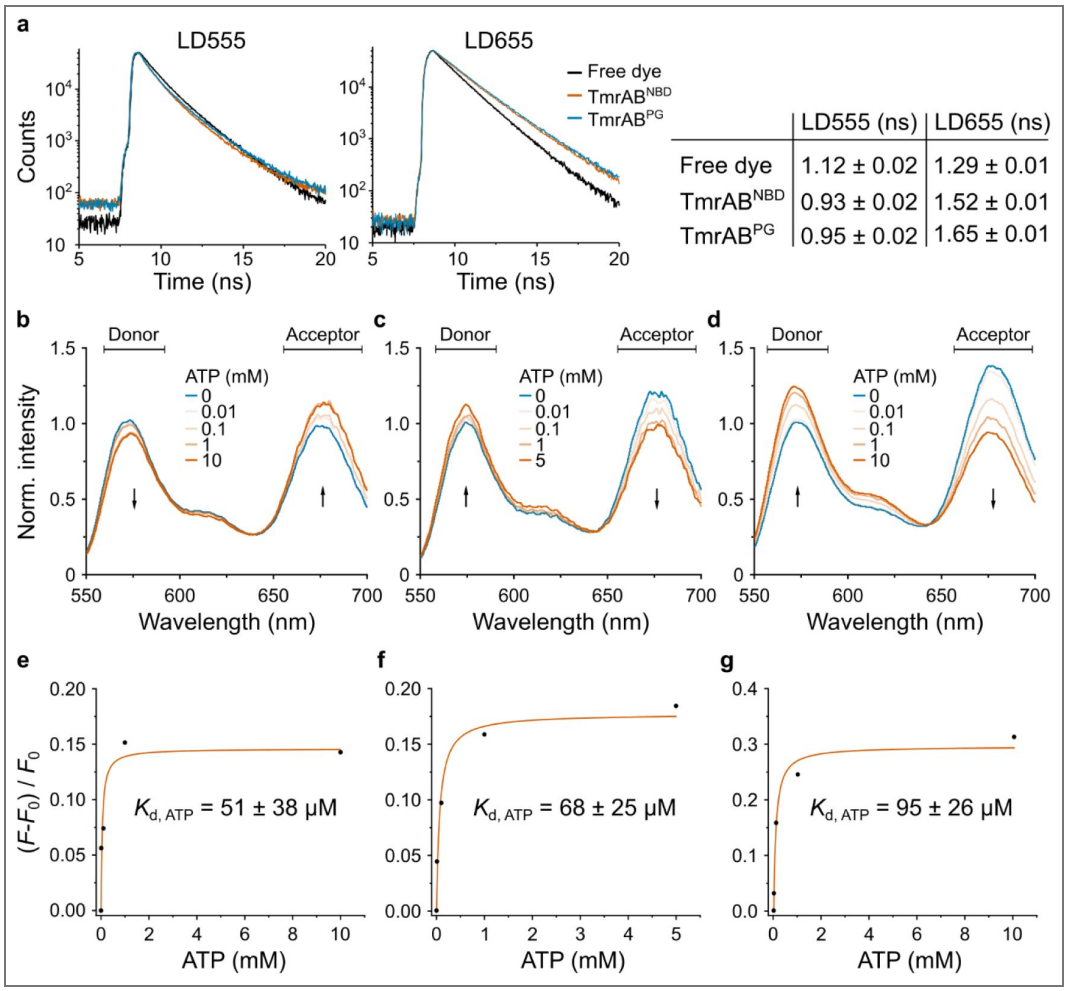

Figure 1 Figure supplement 2. **FRET capabilities of labeled TmrAB variants.**

a, Time-correlated single-photon counting histograms of LD555 (left) and LD655 (middle) measured under three conditions: free dye in buffer (black), LD555/LD655-labeled TmrAB^{NBD} (orange), and LD555/LD655-labeled TmrAB^{PG} (blue). Amplitude-weighted average fluorescence lifetimes are summarized in the table (right), confirming sufficient rotational freedom for reliable FRET measurements. **b–d**, Ensemble donor-exited emission spectra (550–700 nm, excitation 520 nm) of (**b**) TmrAB^{NBD}, (**c**) TmrAB^{PG}, and (**d**) the slow-turnover variant TmrAB^{PG_EQ}, stochastically labeled with LD555/LD655 and incubated with increasing ATP concentrations. Spectra are normalized to donor intensity in the apo state. ATP-dependent donor quenching and acceptor sensitization indicate that all variants retain FRET capability. **e–g**, Fractional fluorescence changes, $(F\text{-}F_0)/F_0$, where F is acceptor emission intensity and F_0 is the intensity in the apo state, plotted as a function of ATP concentration for (**e**) TmrAB^{NBD}, (**f**) TmrAB^{PG}, and (**g**) TmrAB^{PG_EQ}. Data were fitted with a hyperbolic binding model to determine apparent $K_{d,\,ATP}$ values, consistent with ensemble FRET measurements of ATP binding.

marginally affected and, most importantly, identical between the TmrAB variants, indicating dynamics orientational averaging of the transition dipoles and confirming that the labeled constructs are suitable for quantitative FRET studies[32–34].

Ensemble ATP titration (0–10 mM ATP) revealed the expected concentration-dependent donor quenching and acceptor sensitization (Fig. 1–Fig. S2b–d). ATP-induced fractional fluorescence changes provided as a quantitative readout of conformational transitions, allowing estimation of equilibrium dissociation constants for ATP binding ($K_{d,\ ATP}$) to labeled TmrAB variants (Fig. 1–Fig. S2e–g). The measured apparent $K_{d,\ ATP}$ values—51 ± 38 μM for $TmrAB^{NBD}$, 68 ± 25 μM for $TmrAB^{PG}$, and 95 ± 26 μM for the slow-turnover variant $TmrAB^{PG\_EQ}$—are in good agreement with previously reported values (~100 μM for $TmrA^{E523Q}B$)[12], indicating that fluorophore labeling does not perturb ATP binding. Notably, $TmrAB^{PG\_EQ}$ exhibited a larger shift in ATP-induced fluorescence change than $TmrAB^{PG}$, consistent with stabilization of the ATP-bound conformation and reduced catalytic turnover.

ATP-induced conformational switching resolved by single-molecule FRET

TmrAB variants were site-specifically immobilized on PEGylated coverslips using a conformation-independent, TmrB-specific nanobody ($Nb9F10^{S63C}$)[11] conjugated to maleimide-PEG_{11}-biotin (Fig. 2a). Previous studies confirmed that this nanobody does not perturb TmrAB transport or ATPase activity[11,25]. Donor and acceptor photons were recorded by a total-internal reflection fluorescence (TIRF) microscope using alternating laser excitation (ALEX; NanoImager) at 40 °C (Fig. 2b). Single-molecule localization, fluorescence-trajectory extraction, and background correction were performed using NanoImager software, followed by DeepFRET-based machine-learning trace classification and corrections for donor leakage, direct acceptor excitation, and difference in detection-efficiency[17,35,36] (Fig. 2–Fig. S1 and 2). FRET efficiency (E) and stoichiometry (S) were calculated from the corrected fluorescence-trajectories (see Methods, Eq. 1 and Eq. 2).

FRET efficiency (E) histograms revealed two Gaussian populations corresponding to the apo and ATP-bound states (Fig. 2d,e). In the absence of ATP, only the apo population was observed, whereas addition of 3 mM ATP induced the appearance of a second ATP-bound population. For $TmrAB^{NBD}$, the apo and ATP-bound populations exhibited mean E values of 0.58 and 0.88 (ΔE = 0.30), respectively, with ~77% of molecules occupying the ATP-bound state. For $TmrAB^{PG}$, mean E values were 0.97 (apo) and 0.86 (ATP-bound) (ΔE = 0.11), with ~80% of molecules in the ATP-bound state.

Distance estimates calculated using a Förster radius of R_0 = 63.5 Å (ref.[37]) yielded apparent distances of 60.2 Å (apo) and 45.6 Å (ATP-bound) for $TmrAB^{NBD}$, and 35.6 Å (apo) and 46.9 Å (ATP-bound) for $TmrAB^{PG}$. For $TmrAB^{NBD}$, the experimentally derived ΔR of 14.6 Å closely agreed with the AV simulations. In contrast, the smaller ΔR of 11.4 Å observed for $TmrAB^{PG}$ deviated from simulated values, indicating that the ATP-bound population at this site represents a mixture of rapidly interconverting conformations rather than a single well-defined state.

To assess the ATP sensitivity, we quantified conformational responses across a wide range of ATP concentrations, spanning well below the reported $K_{d,\ ATP}$ (~100 μM for $TmrA^{E523Q}B$)[12] up to physiologically relevant levels (3 mM ATP). smFRET measurements revealed dose-dependent population shifts: $TmrAB^{NBD}$ transitioned from a low-FRET apo state (E = 0.58) to high-FRET ATP-bound state (E = 0.88), whereas $TmrAB^{PG}$ shifted from a high-FRET apo state (E = 0.97) to a lower-FRET ATP-bound state (E = 0.86) (Fig. 3a,c). Langmuir isotherm fits yielded $K_{d,\ ATP}$ values of 13 ± 1 μM for $TmrAB^{NBD}$ and 2 ± 1 μM for $TmrAB^{PG}$ (Fig. 3b,d), indicating saturation at ATP concentrations well below physiological levels (3 mM). For the $TmrAB^{PG}$ variant, population quantification and subsequent determination of $K_{d,\ ATP}$ are unreliable due to insufficient separation of the two FRET populations below 1 mM ATP, consistent with the smaller ΔE observed for this labeling configuration.

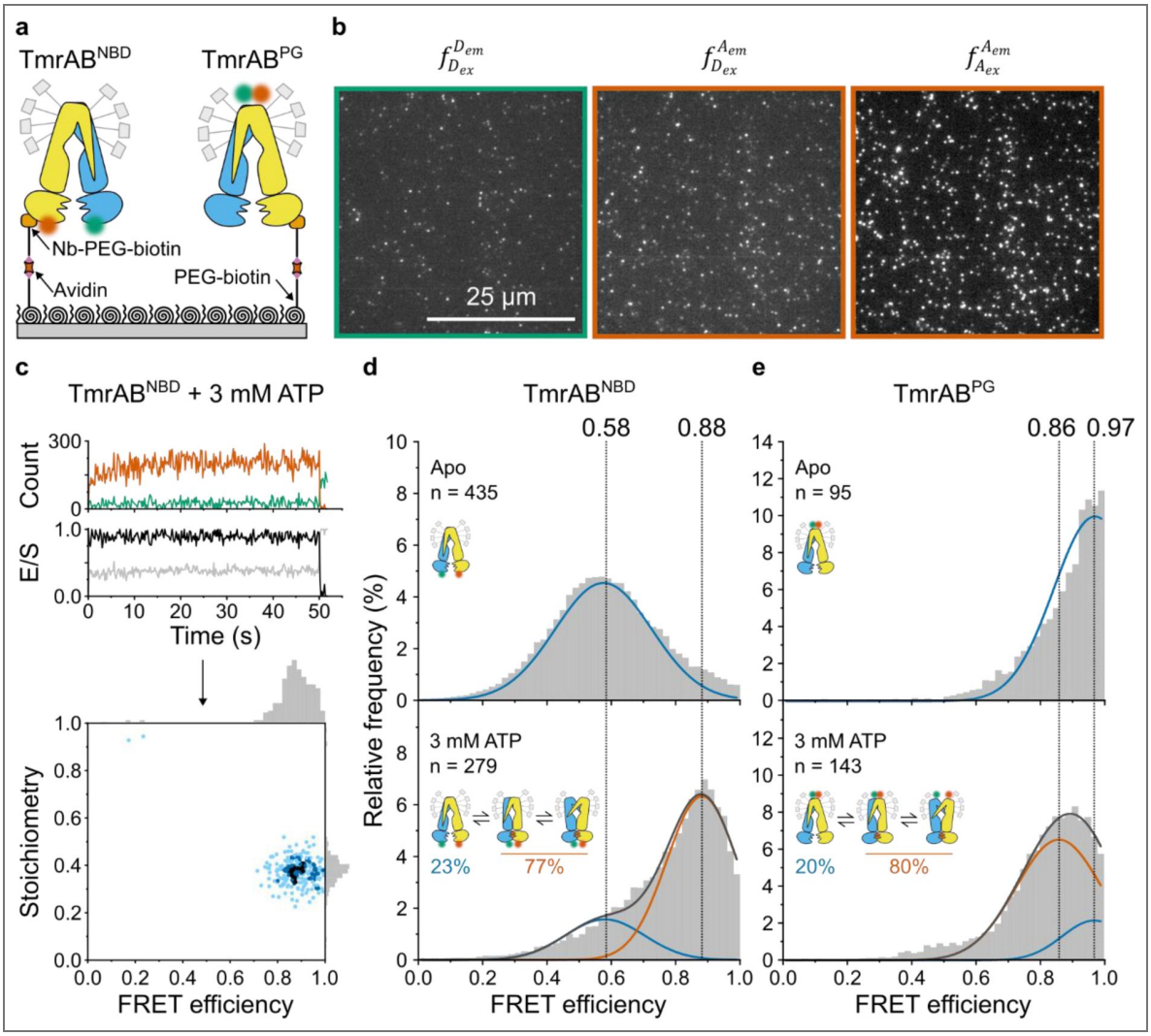

Figure 2. ATP-induced conformational changes of TmrAB analyzed by smFRET.

a, Experimental setup. TmrAB^{NBD} (left) and TmrAB^{PG} (right) variants were labeled with LD555/LD655 and tethered to PEGylated coverslips via a biotinylated anti-TmrB nanobody (Nb9F10^{S63C}). **b**, smFRET imaging. Samples were recorded using total internal reflection fluorescence (TIRF) microscopy with alternating laser excitation (ALEX; donor: 532 nm; acceptor: 640 nm). Emission was collected in two channels (donor: 498-620 nm; acceptor: 662-710 nm). Donor fluorescence ($f_{D_{ex}}^{D_{em}}$ donor excitation at donor emission), sensitized acceptor fluorescence ($f_{D_{ex}}^{A_{em}}$ donor excitation at acceptor emission), and direct acceptor fluorescence ($f_{A_{ex}}^{A_{em}}$ acceptor excitation at acceptor emission) were used to calculate FRET efficiency (*E*) and stoichiometry (*S*). Fluorescence time traces were analyzed with DeepFRET[35]. **c**, Representative TmrAB^{NBD} trace in ATP-bound state (top) and corresponding FRET efficiency/stoichiometry plot (bottom). Donor emission upon donor excitation is shown in green as the number of detected photons per frame (counts), acceptor intensity upon donor excitation in orange, FRET efficiency (*E*) in black, and stoichiometry (*S*) in grey. The slight increase in donor fluorescence observed during the first seconds of acquisition reflects photophysical equilibration of the fluorophore and instrumental stabilization and does not affect FRET efficiency or stoichiometry, which are ratio-based and remain constant over time[17]. **d**,**e**, Population analysis. FRET efficiency (*E*) histograms for (**d**) TmrAB^{NBD} and (**e**) TmrAB^{PG} are shown for the apo state (top) and ATP-bound state (bottom; 3 mM ATP). Histograms were fitted with two Gaussian populations corresponding to the apo state (blue; defined from apo measurements) and the ATP-bound state (orange; defined from two-component fits at saturating ATP). Dotted vertical lines indicate mean *E* values of each population. Population fractions, calculated from Gaussian areas, are summarized schematically in each panel.

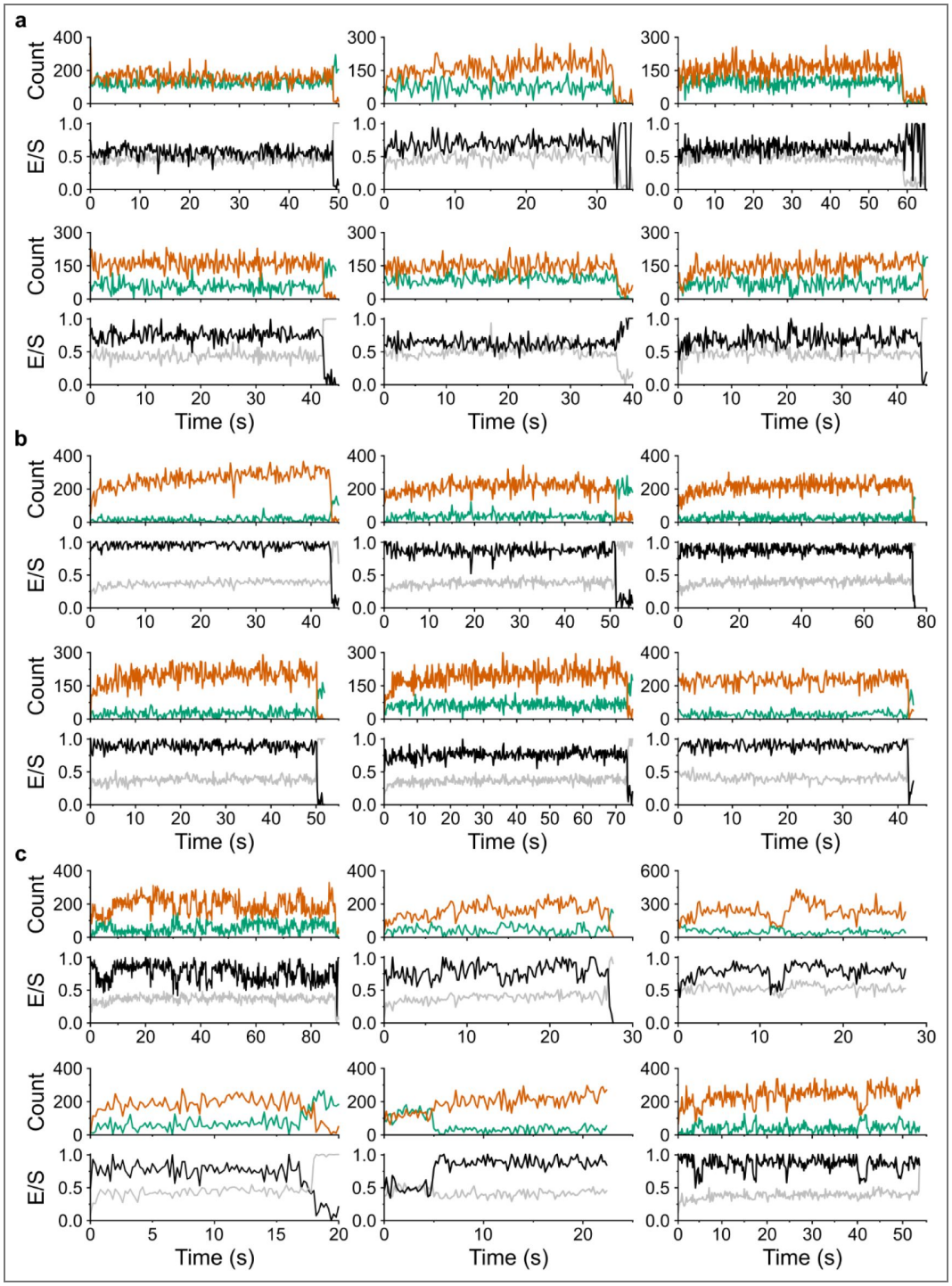

Figure 2 Figure supplement 1. Representative smFRET traces of TmrAB^{NBD}.

Representative single-molecule FRET (smFRET) traces of TmrAB^{NBD} were recorded (**a**) in the ATP-free state and (**b, c**) in the presence of 3 mM ATP. Hidden Markow modeling (HMM) was applied to classify traces into (**b**) static and (**c**) dynamic, based on the absence or presence of transitions between ATP-free and ATP-bound conformational states. Donor fluorescence intensity upon donor excitation is shown in green, acceptor fluorescence intensity upon donor excitation in orange, FRET efficiency (*E*) in black, and stoichiometry (*S*) in grey.

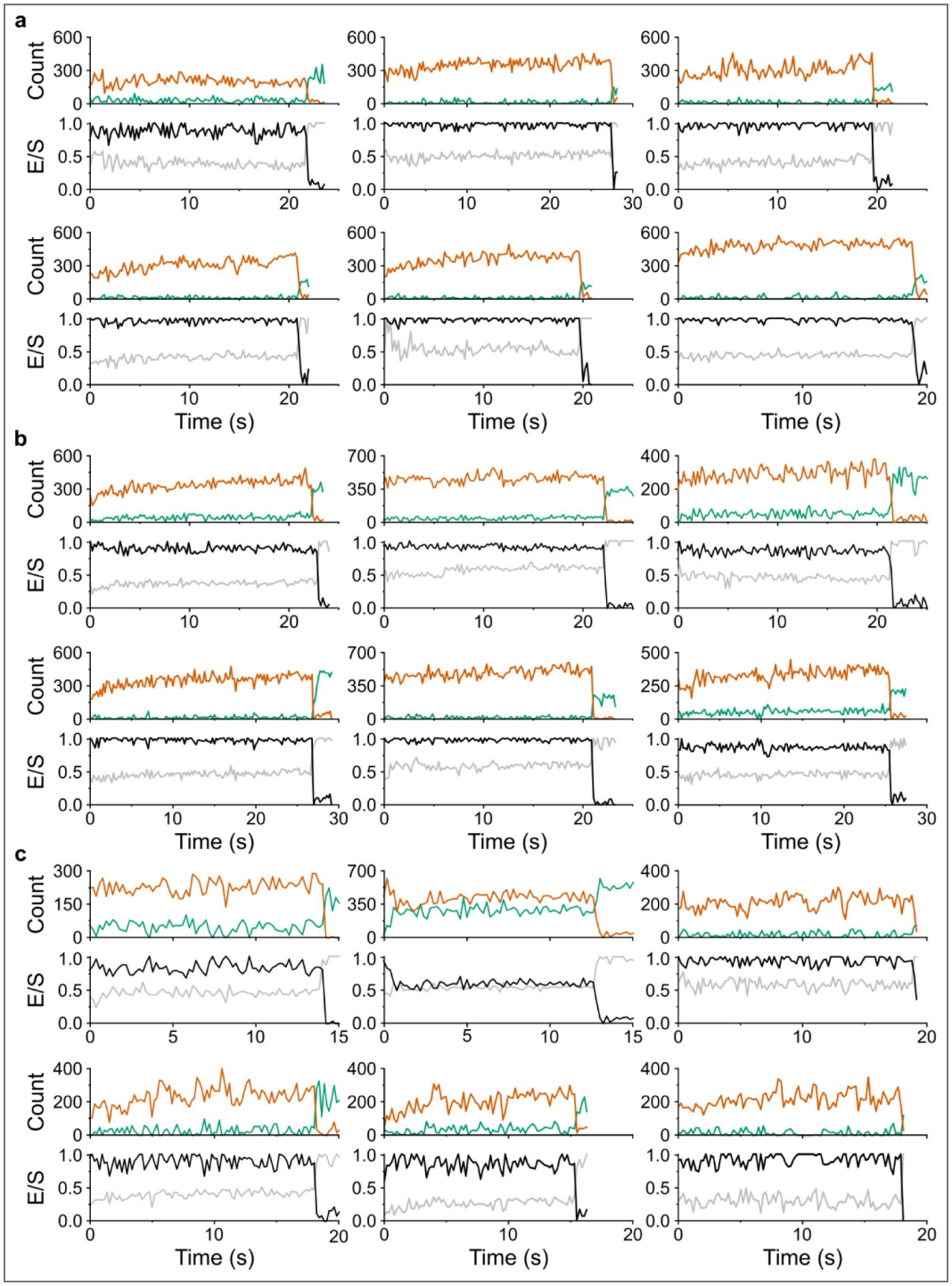

Figure 2 Figure supplement 2. Representative smFRET traces of TmrAB^{PG}.

Representative single-molecule FRET (smFRET) traces of TmrAB^{PG} were recorded (**a**) in the ATP-free state and (**b, c**) in the presence of 3 mM ATP. Hidden Markow modeling (HMM) was applied to classify traces into (**b**) static and (**c**) dynamic, based on the absence or presence of transitions between ATP-free and ATP-bound conformational states. Donor fluorescence intensity upon donor excitation is shown in green, acceptor fluorescence intensity upon donor excitation in orange, FRET efficiency (*E*) in black, and stoichiometry (*S*) in grey.

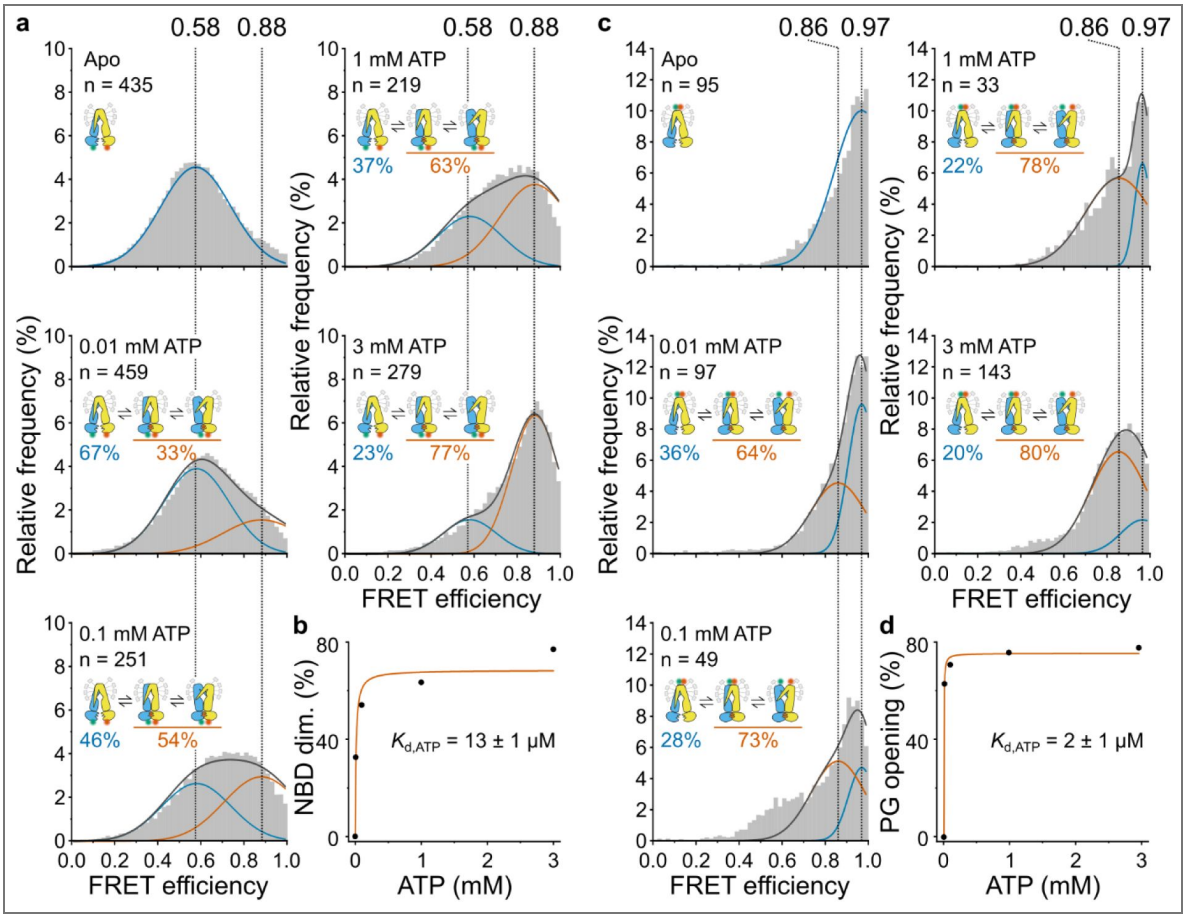

Figure 3. ATP-dependent shifts in smFRET populations of TmrAB.

a,**c**, Increasing ATP concentrations gradually redistributed the population between apo and ATP-bound conformations for (**a**) $TmrAB^{NBD}$ and (**c**) $TmrAB^{PG}$. FRET efficiency (*E*) histograms were fitted with two Gaussian populations corresponding to the ATP-free state (blue: defined from apo samples) and the ATP-bound state (orange; determined from fits at saturating ATP). Dotted vertical lines indicate the mean *E* values of each population. Relative proportion fractions, calculated from Gaussian areas, are summarized schematically in each panel. **b**,**d**, ATP-binding curves were obtained by plotting the fraction of molecules in the ATP-bound states as a function of ATP concentration for (**b**) $TmrAB^{NBD}$ (reporting NBD dimerization) and (**d**) $TmrAB^{PG}$ (reporting PG opening). Data were fitted with a Langmuir isotherm to determine the apparent dissociation constant $K_{d,\ ATP}$ of each variant.

Trapping of TmrAB^{PG} reveals a previously hidden outward-facing open state

At physiological ATP concentrations (3 mM), ~80% of TmrAB^{PG} molecules populated the ATP-bound state (E = 0.86), closely matching the ATP-bound population (~77% of NBD-dimerized) observed for TmrAB^{NBD} (Fig. 3). This agreement indicates that both labeling strategies consistently report ATP-dependent conformational changes. However, the ATP-induced shift observed for the periplasmic-gate reporter TmrAB^{PG} (ΔE = 0.11, ΔR = 11.4 Å; Fig. 3c) was substantially smaller than predicted by AV simulations (ΔE = 0.27, ΔR = 23.2 Å; Fig. 1c). This discrepancy indicates that the ATP-bound population at E = 0.86 represents an unresolved ensemble, potentially comprising OF^{open} and OF^{occluded} conformations, as well as the post-hydrolysis asymmetric unlocked return states (UR^{asym} and UR^{asym}*), which are clearly indistinguishable from OF^{occluded} within the current FRET geometry[11].

To test whether these states are kinetically unresolved by smFRET, we applied three complementary strategies to arrest the OF^{open} conformation of TmrAB^{PG}: (i) a slow-turnover catalytic mutant (TmrAB^{PG_EQ}), (ii) Mg^{2+} depletion using EDTA, and (iii) reverse inhibition by high concentrations of the substrate peptide RRYQKSTEL (R9L) (Fig. 4). Slow-turnover variants have previously enabled structural separation of OF^{open} and OF^{occluded} states[11,12,14,25]. Mg^{2+} depletion blocks ATP hydrolysis while preserving ATP binding, allowing rapid and reversible trapping[25]. We further hypothesized that trans-inhibition by peptide binding sterically restricts PG closure and is therefore expected to stabilize OF^{open} in a dose-dependent manner[26,27].

In conditions lacking ATP, either in the absence of nucleotides or in the presence of ADP (3 mM ADP), the slow-turnover variant TmrAB^{PG_EQ} populated a single high-FRET state (E = 0.97) (Fig. 4a, top and middle). These results indicate that ADP binding alone is insufficient to promote NBD dimerization nor PG opening, consistent with previous biochemical and structural observations[11,12]. Upon ATP addition (3 mM ATP), however, the conformational landscape diverged sharply from that of wild-type TmrAB^{PG}. Instead of the two-state distribution observed for wild-type (apo: E = 0.97, ~20%; ATP-bound: E = 0.86, ~80%) (Fig. 2e, bottom), TmrAB^{PG_EQ} exhibited three well-resolved populations with mean E values of E = 0.97 (~14%), E = 0.86 (~55%), and E = 0.63 (~31%) (Fig. 4a, bottom).

As in wild-type TmrAB^{PG}, the high-FRET population (E = 0.97) corresponds to the IF state, whereas the intermediate-FRET population (E = 0.86) likely represents a dynamic equilibrium of OF^{open} and OF^{occluded} conformations, as suggested by cryo-EM analyses[11]. Post-hydrolysis return states (UR^{asym} and UR^{asym}*) are expected to be minimally populated in TmrAB^{PG_EQ} due to its drastically reduced ATP hydrolysis rate[12]. Notably, the low-FRET ATP-bound population (E = 0.63) was entirely absent in wild-type. The transition from E = 0.97 to E = 0.63 corresponds to ΔE = 0.34 and ΔR = 22.5 Å, in close agreement with the IF◊OF^{open} distance predicted by AV simulations (ΔR = 23.2 Å; Fig. 1), thereby postulating E = 0.63 as the OF^{open} conformation.

Mg^{2+} depletion independently reproduced this three-state landscape. In the absence of Mg^{2+}, wild-type TmrAB^{PG} transitioned from a single apo population (without ATP; E = 0.97) (Fig. 4b, top) to three ATP-bound populations (3 mM ATP; E = 0.97, ~13%; E = 0.86, ~56%; E = 0.63, ~31%) (Fig. 4b, middle) closely resembling those observed for the slow-turnover variant (Fig. 4a, bottom). Reintroducing Mg^{2+} abolished the E = 0.63 population and restored the wild-type two-state distribution (Fig. 4b, bottom). This reversibility confirmed that the ATP-bound OF^{open} state (E = 0.63) is selectively revealed only when ATP hydrolysis is prevented.

Finally, we tested whether periplasmic substrate binding shifts the conformational equilibrium of wild-type TmrAB^{PG} toward OF^{open}. In the presence of ATP (3 mM), increasing concentrations of peptide substrate (0.3–2 mM R9L) progressively enriched the E = 0.63 population from ~20% to ~38% (Fig. 4c). This dose-dependent stabilization mirrors trans-inhibition behavior reported for human TAP1/2 and reflects the upper substrate-loading capacity of the transporter[26].

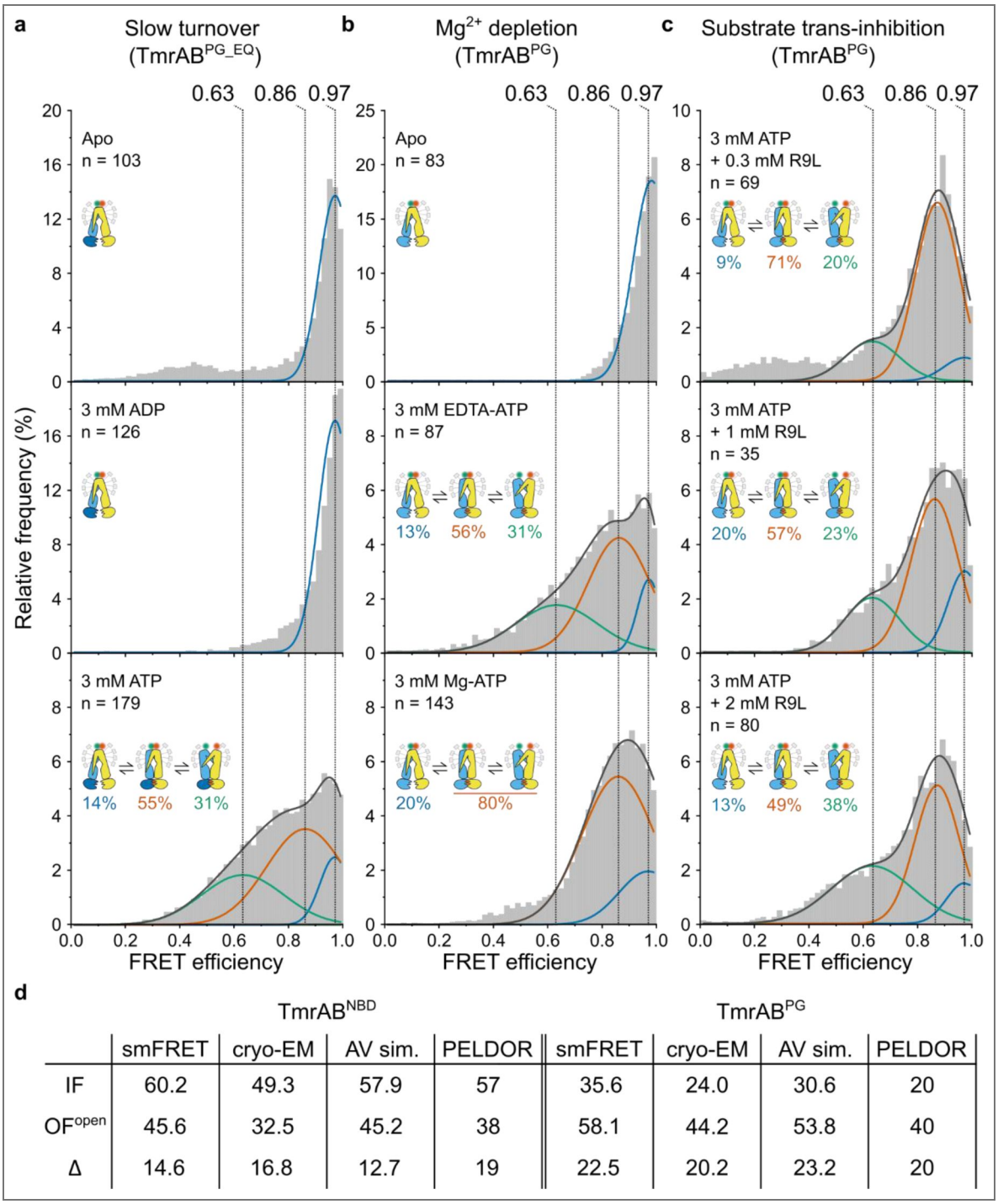

d

	TmrAB^{NBD}				TmrAB^{PG}			
	smFRET	cryo-EM	AV sim.	PELDOR	smFRET	cryo-EM	AV sim.	PELDOR
IF	60.2	49.3	57.9	57	35.6	24.0	30.6	20
OF^{open}	45.6	32.5	45.2	38	58.1	44.2	53.8	40
Δ	14.6	16.8	12.7	19	22.5	20.2	23.2	20

Figure 4. Identification of the outward-facing open (OF^{open}) conformation.

a–c, Three complementary approaches were employed to resolve OF^{open} state: (**a**) the slow-turnover variant TmrAB^{PG_EQ}, (**b**) imaging in Mg^{2+}-free buffer supplemented with EDTA, and (**c**) stabilizing via reverse inhibition using high concentrations of peptide substrate. FRET efficiency (*E*) histograms were fitted with three Gaussian populations corresponding to the ATP-free state (blue), the ATP-bound state (orange), and the stabilized OF^{open} state (green). All three strategies revealed a distinct OF^{open} population. Dotted vertical lines indicate the mean *E* values of each population. Relative proportion fractions, calculated from Gaussian areas, are summarized schematically in each panel. **d**, Comparison of inter-residues distances. Distances (Å) between selected residues on the NBDs and PG of TmrAB were determined by multiple methods: smFRET values (this study) for detergent-solubilized TmrAB; cryo-EM distances (C_β–C_β) from nanodisc-reconstituted TmrAB (PDB 6RAH, 6RAN)[11]; accessible-volume (AV) simulation distances for nanodisc-reconstituted TmrAB (this study); and PELDOR/DEER distances from detergent-solubilized TmrAB[15].

Distance changes derived from smFRET closely match AV simulations, cryo-EM structures (PDB 6RAH, 6RAN)[11], and DEER/PELDOR measurements[14] (Fig. 4d), together validating assignment of the E = 0.63 population as the OF^{open} conformation.

Kinetics and thermodynamics of the transport cycle

ALEX-smFRET data were acquired with an effective temporal resolution of 200 ms (100 ms per excitation channel). Shorter integration times compromised the signal-to-noise ratio and precluded reliable FRET determination. To quantify conformational dynamics, we applied Hidden Markov Modeling (HMM) using MASH-FRET[38], classifying traces as either static (single FRET state) or dynamic (multiple states). Approximately 95% of traces in each condition were classified as static, indicating that most conformational transitions occur at or below our temporal resolution.

Although individual transitions could not be directly resolved, population-based analysis (Fig. 3), combined with biochemical turnover measurements (Fig. 1–Fig. S1c), allowed estimation of ATP-bound dwell times. At saturating ATP conditions well above the apparent $K_{d,\ ATP}$ (3 mM, 40 °C), wild-type TmrAB exhibited a catalytic turnover rate of k_{cat} = 2.57 ± 0.38 s^{-1} (Fig. 1–Fig. S1c), corresponding to a full transport cycle time (τ_{cycle}) of 395 ± 55 ms. ATP-bound dwell times (τ_d) were derived from population ratios obtained from Gaussian fits of the FRET efficiency histograms (Fig. 3; see Methods, Eq. 3 and Eq. 4). These analyses yielded ATP-bound dwell times of 304 ± 43 ms for $TmrAB^{NBD}$ (~77% ATP-bound) and 316 ± 44 ms for $TmrAB^{PG}$ (~80% ATP-bound), with the remaining ATP-free intervals (~20–23%) accounting for 91 ms and 79 ms of the cycle, respectively.

Together, these measurements establish a quantitative, single-molecule description of conformation state occupancies and dwell times throughout the catalytic cycle of a heterodimeric ABC transporter under active turnover conditions, providing valuable insights into the dynamic landscape of its translocation cycle.

Discussion

smFRET has become an indispensable tool for dissecting conformational dynamics of membrane proteins, including receptors, ion channels, and transporters, by directly linking structural transitions to functional states With the ABC transporter family, however, smFRET studies have largely been confined to monomeric or homodimeric systems[22–24], leaving the dynamic behavior of asymmetric, heterodimeric transporter comparatively unexplored. Here, we apply smFRET to the heterodimeric type IV ABC transporter TmrAB, extending single-molecule analysis to an asymmetric transporter system and uncovering dynamic features of the transport cycle that are inaccessible to ensemble-averaged approaches.

By positioning FRET reporters at the nucleotide-binding domains (NBDs) and periplasmic gate (PG), we directly monitored ATP-dependent coupling between chemical energy input and global conformational rearrangements. Importantly, these structural rearrangements are not strictly correlated: NBD dimerization can give rise to either an outward-facing open (OF^{open}) or occluded ($OF^{occluded}$) conformation[11,12]. This decoupling underscores the need to monitor both cytosolic and periplasmic regions to resolve the transport mechanism.

Labeling sites previously validated for PELDOR/DEER spectroscopy[10,14,15] were adapted for smFRET and rigorously benchmarked using accessible-volume (AV) simulations[30], fluorescence lifetime analysis, and ensemble FRET titrations. This additional validation is essential because fluorophores impose stricter steric and rotational constraints than nitroxide spin labels[32]. Collectively, these controls demonstrate that fluorophore attachment preserves native-like conformational behavior and ATP binding, establishing TmrAB as a robust system for quantitative single-molecule analysis. Consistent with this conclusion, fluorescence lifetime analysis showed no evidence for substantial protein-fluorophore quenching or restricted dye motion, as indicated by donor lifetime shortening and prolonged acceptor lifetimes characteristic of efficient energy transfer[17].

Single-molecule measurements resolved two dominant FRET populations corresponding to apo and ATP-bound states for both reporter variants TmrAB^{NBD} and TmrAB^{PG}. ATP titrations spanning concentrations well below the reported apparent $K_{d,\ ATP}$ (~100 μM for TmrA^{E523Q}B)[12] up to physiologically relevant levels (3 mM ATP) revealed gradual, concentration-dependent shifts between these populations, demonstrating the high sensitivity of the FRET constructs to ATP binding. Notably, apparent $K_{d,\ ATP}$ values derived from smFRET (2–13 μM) were substantially lower than those obtained from ensemble FRET measurements (50–100 μM). This difference likely reflects the inherent selectively of single-molecule analyses for properly folded and catalytically competent transporters. In smFRET experiments, aggregated or inactive species can be identified and excluded during trace selection based on fluorescence intensity, stoichiometry, and photobleaching behavior, thereby enriching the analyzed population for functional molecules.

Crucially, the ATP-bound population may reflect a rapidly interconverting ensemble of conformations, rather than a single static structure, potentially including OF^{open}, OF^{occluded}, and post-hydrolysis unlocked return states (UR^{asym} and UR^{asym*}). These transitions occur faster than the ~200 ms temporal resolution of our measurements, resulting in averaged FRET efficiencies under turnover conditions. Using three independent trapping strategies—slow-turnover catalysis, Mg^{2+} depletion, and substrate trans-inhibition—we stabilized and directly resolved a previously hidden OF^{open} conformation. The associated distance changes are generally consistent with cryo-EM structures[11], PELDOR/DEER data[10,14,15], and simulation-based predictions, suggesting that detergent-solubilized TmrAB samples a largely native-like conformational landscape.

Although detergent-solubilized and lipid nanodisc-reconstituted TmrAB exhibit similar global conformational states, the conformational space accessible to attached fluorophores may be differentially influenced by membrane-associated environments[19,39,40]. In particular, fluorophores attached near the periplasmic gate may experience steric restrictions due to partial overlap with the membrane region, as suggested by AV simulations. While such effects are negligible under the detergent conditions used here, they should be carefully evaluated in future studies employing membrane-embedded systems. Single-molecule measurements further revealed that addition of the peptide substrate induces concentration-dependent shifts in the conformational equilibrium. Increasing substrate concentrations progressively stabilized the OF^{open} state, consistent with trans-inhibition behavior observed in human TAP1/2[26] and bovine ABCC1[27], and reflecting the finite substrate-loading capacity of the transporter[26].

Quantitative deconvolution of FRET populations enabled direct determination of conformational state occupancies under physiological ATP concentrations. During active turnover, TmrAB populates the IF state (~20%), the OF^{open} state (~25%), and OF^{occluded}/post-hydrolysis states (UR^{asym} and UR^{asym*}) (~55%) (Fig. 5). The current reporter geometries do not allow direct discrimination between OF^{occluded} and post-hydrolysis states because fluorophores were placed at the noncanonical nucleotide-binding site. However, contributions from post-hydrolysis states are expected to be minimal for slow-turnover TmrAB variant (TmrAB^{PG_EQ}), owing to its drastically reduced ATP hydrolysis rate. To our knowledge, this represents the first single-molecule quantification of conformational equilibria for a heterodimeric ABC transporter under catalytic conditions. While these distributions broadly align with cryo-EM particle classifications[11,25], smFRET resolves fewer IF states than the cryo-EM distinction between IF^{wide} and IF^{narrow}, and additionally captures ATP-bound intermediates that are challenging to resolve structurally due to rapid interconversion.

All smFRET measurements were performed at 40 °C to maintain consistency with prior biochemical studies and ensure fluorophore stability. At the physiological temperature of *T. thermophilus* (68 °C), absolute rates of ATP turnover and conformational transitions are expected to increase, although relative state occupancies may remain conserved if the underlying free-energy landscape is preserved. Despite a substantial fraction of static single-molecule trajectories, ATP-dependent population shifts and catalytic rates indicate that TmrAB operates near the temporal resolution limit of our measurements. Integrating smFRET-derived state occupancies with biochemical turnover rates yields an ATP-bound dwell time of approximately 300 ms, in good agreement with previous biochemical estimates[9,12].

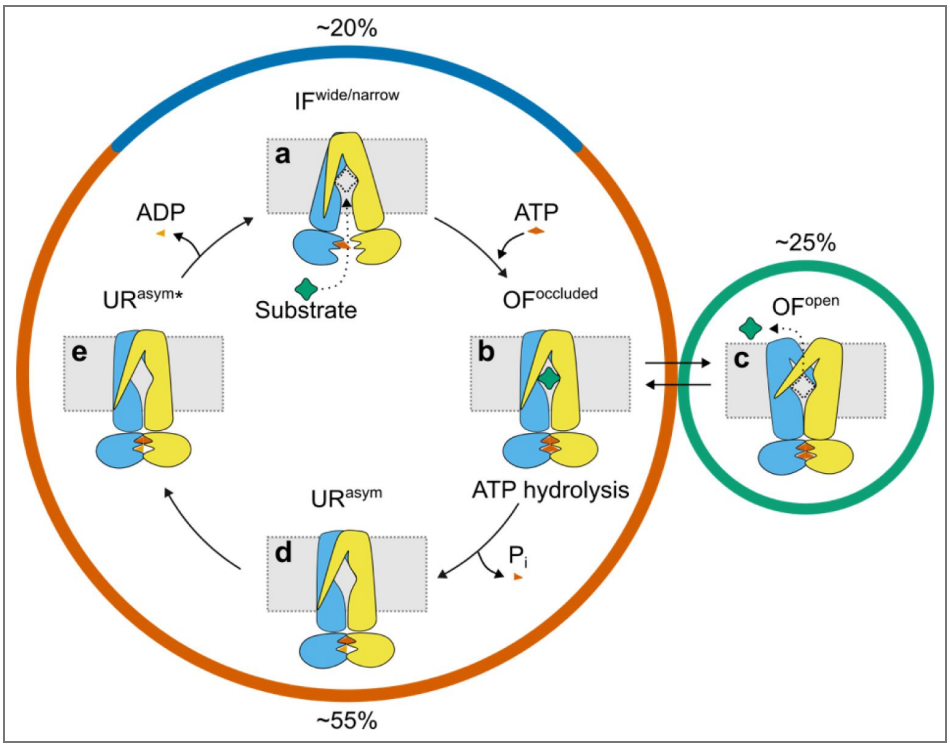

Figure 5. Conformational state distribution and catalytic cycle of TmrAB under active turnover.

Schematic of the TmrAB transport cycle summarizing major conformational states and their estimated population distributions under physiological ATP concentrations (3 mM, 40 °C). **a**, The inward-facing apo state (IF^{narrow} and IF^{wide}; blue arc) accounts for ~20% of molecules and is characterized by separated NBDs and a cytosol-accessible substrate-binding cavity. Substrate binding stabilizes the IF^{wide} conformation[11]. Independent of substrate, ATP binding induces NBD dimerization and transition to the ATP-bound ensemble. **b**,**c**, Under substrate-bound turnover conditions, TmrAB proceeds via the (**b**) $OF^{occluded}$ to (**c**) OF^{open} state in which the substrate release occurs. Under steady-state turnover, the ATP-bound ensemble rapidly interconverts between substrate-free $OF^{occluded}$ and OF^{open} accounting for ~25% of the ATP-bound population (green circle). These transitions occur faster than the ~200 ms temporal resolution of standard smFRET measurement, resulting in an averaged signal under turnover conditions. $OF^{occluded}$ likely serves as an obligate intermediate between IF and OF^{open}, preventing substrate backflow by maintaining a substrate-binding cavity occluded during the structural rearrangements of the PG and NBDs. Although a substrate-bound $OF^{occluded}$ state has not been directly observed for TmrAB, its existence is supported by structures of the homodimeric type IV transporter BmrA[46]. Reduced ATP hydrolysis or substrate trans-inhibition enables trapping of the transporter in the $OF^{open.}$ state. **d**,**e**, ATP hydrolysis and phosphate (P_i) release generate post-hydrolysis return states: (**d**) UR^{asym} and (**e**) UR^{asym}*. Subsequent ADP release restores the apo IF conformation, completing the transport cycle. Overall, the ATP-bound phase (**b–e**) represents ~55% occupancy (orange arc) with an estimated dwell time of ~310 ms, whereas the apo/ATP-rebinding phase (**a**) lasts ~90 ms, yielding a total cycle time of ~400 ms (k_{cat} = 2.57 s^{-1}). TmrA is shown in blue, TmrB in yellow, substrate as a green diamond, and nucleotides as orange symbols. Dotted grey boxes indicate the approximate position of the NBD dimer interface.

Emerging microsecond-resolution smFRET approaches offer the potential to directly visualize short-lived intermediates within the transport cycle[41]. Future studies could further benefit from three- or four-color FRET strategies[42,43], which would allow simultaneous monitoring of multiple structural elements. In particular, dual labeling of the NBDs and PG could provide direct detection of the $OF^{occluded}$ state, while probes placed at both canonical and noncanonical nucleotide-binding sites could capture post-hydrolysis conformational dynamics.

In summary, this work establishes smFRET as a powerful approach for mapping the dynamic landscape of asymmetric ABC transporters. By quantitatively linking ATP binding, conformational equilibria, and kinetics at the single-molecule level, our study resolved an important aspect of the transport mechanism how chemical energy is transduced into directional transport in heterodimeric ABC systems. Integration of native lipid environments, higher temporal resolution, and substrate engagement will further illuminate the coordination of ATP hydrolysis and substrate translocation during transport.

Methods

Expression, purification, and labeling of TmrAB

His_{10}-tagged TmrAB variants were expressed in *E. coli* BL21(DE3) (Thermo Fisher Scientific) as described previously[12]. Cells were grown in high-salt LB media (Carl Roth) supplemented with 100 µg ml^{-1} ampicillin (PAA Laboratories) at 37 °C. At an OD_{600} of 0.5, expression was induced with 1 mM isopropyl β-D-thiogalactopyranoside (IPTG; Carl Roth), and cultures were incubated for 3 h at 37 °C. Cells were harvested by centrifugation (4,500 × *g*, 4 °C, 15 min) and stored at –80 °C.

For purification, cell pellets were resuspended in lysis buffer (20 mM HEPES-NaOH pH 7.5, 300 mM NaCl, 50 µg ml^{-1} lysozyme, 0.2 mM phenylmethylsulfonyl fluoride (PMSF)) and lysed by sonication. Cell debris was removed by centrifugation (18,000 × *g*, 4 °C, 35 min), and membranes were collected by ultracentrifugation (100,000 × *g*, 4 °C, 30 min). Membranes were solubilized for 2 h at 4 °C in purification buffer (20 mM HEPES-NaOH pH 7.5, 300 mM NaCl) containing 20 mM n-dodecyl β-D-maltoside (β-DDM; Carl Roth). After ultracentrifugation (100,000 × *g*, 30 min, 4 °C), the supernatant was incubated with Ni-NTA agarose (Bio-Rad) for 1 h at 4 °C. The resin was washed with 20 column volumes of wash buffer (20 mM HEPES-NaOH pH 7.5, 300 mM NaCl, 1 mM β-DDM) containing 50 mM imidazole, and TmrAB was eluted with elution buffer (20 mM HEPES-NaOH pH 7.5, 300 mM NaCl, 1 mM β-DDM, 300 mM imidazole).

For fluorophore labeling, TmrAB variants were conjugated via maleimide chemistry using LD555 and LD655 (Lumidyne Technologies). Labeling was carried out at a 1:10:10 molar ratio of protein to each dye in elution buffer for 3 h at 4 °C. Excess dye was quenched with 2 mM β-mercaptoethanol (Sigma-Aldrich), and the labeled protein was buffer-exchanged into size-exclusion chromatography (SEC) buffer (20 mM HEPES-NaOH pH 7.5, 150 mM NaCl, 1 mM β-DDM) using a Zeba Spin Desalting Column (Thermo Fisher Scientific). Unreacted fluorophores were removed by SEC on a Superdex 200 Increase 10/300 GL column (Cytiva). Labeling efficiency was determined by analytical SEC (Superdex 200 Increase 3.2/300; Cytiva) by monitoring absorbance at 280, 555, and 655 nm. To preserve sample integrity for smFRET measurements, TmrAB was purified and labeled within a single day, stored on ice, and imaged over the following two days.

Time-correlated single-photon counting (TCSPC)

Fluorescence lifetime measurements were performed using a FluoTime 100 spectrometer (PicoQuant) equipped for time-correlated single-photon counting (TCSPC). Experiments were carried out on labeled TmrAB in SEC buffer (20 mM HEPES-NaOH pH 7.5, 150 mM NaCl, 1 mM β-DDM). LD555 and LD655 were excited at 510 nm and 610 nm, respectively. Emission was collected using a 620/60 nm bandpass filter for LD555 and a BG4 700 nm long-pass filter for LD655. Photon arrival times were accumulated until the TCSPC histogram reached a peak count of 50,000 photons. Fluorescence decay curves were analyzed by fitting mono- or bi-exponential decay models using FluoFit software (PicoQuant) and amplitude weighted average of fluorescence lifetime was calculated.

Nanobody production and purification

The nanobody Nb9F10^{S63C} was expressed and purified as described previously[11]. Briefly, Nb9F10^{S63C} was produced in *E. coli* BL21(DE3) cells grown in Terrific Broth (TB; Carl Roth) supplemented with 100 µg ml^{-1} ampicillin at 37 °C. At an OD_{600} of 0.6, expression was induced with 1 mM IPTG, followed by overnight incubation at 28 °C. Cells were harvested by centrifugation (4,500 × *g*, 4 °C, 15 min) and stored at –80 °C. For purification, cell pellets were resuspended in nanobody lysis buffer (25 mM HEPES-NaOH pH 7.4, 300 mM NaCl, 15 mM imidazole, 0.5 mM PMSF) and disrupted by sonication. Cell debris was removed by centrifugation (18,000 × *g*, 4 °C, 35 min), and the clarified lysate was applied to Ni-NTA agarose equilibrated in potassium phosphate (KP_i) buffer (25 mM KP_i pH 6.5, 100 mM KCl, and 0.5 mM tris(2-carboxyethyl) phosphine (TCEP)). Bound nanobody was washed with 10 column volumes (CV) of KP_i buffer and eluted with 8 CV of elution buffer (25 mM KP_i pH 6.0, 20 mM KCl, 300 mM imidazole, 0.5 mM TCEP). Eluted fractions were pooled and further purified by cation exchange chromatography (CEX) on a HiTrap SP column (Cytiva) using a linear gradient from low-salt buffer (25 mM KP_i pH 6.0, 20 mM KCl, 0.5 mM TCEP) to high-salt buffer (25 mM KP_i pH 6.0, 500 mM KCl, 0.5 mM TCEP). The purified nanobody was concentrated and buffer-exchanged into nanobody SEC buffer (20 mM HEPES-NaOH pH 7.5, 150 mM NaCl) using Zeba spin desalting columns, followed by SEC (Superdex 200 Increase 10/300 GL; Cytiva). For site-specific conjugation, Nb9F10^{S63C} was incubated with a biotin-PEG_{11}-maleimide linker (Sigma-Aldrich) at a 1.2:1 molar ratio of protein to linker in the presence of 0.5 mM TCEP for 2 h at 4 °C. Excess linker was removed by desalting on Zeba Spin Desalting Columns, followed by a final SEC step (Superdex 200 Increase 10/300 GL).

SDS-PAGE

The purity of TmrAB samples was assessed by SDS-PAGE. Resolving gels (12%) were prepared using 12% (w/v) acrylamide, 0.5 M Tris-HCl (pH 8.8), 0.13% (w/v) SDS, 0.05% (w/v) ammonium persulphate (APS), and 0.25% (v/v) *N,N,N',N'*-tetramethylethylenediamine (TEMED). Stacking gels contained 4.3% (w/v) acrylamide, 0.5 M Tris/HCl (pH 6.8), 0.09% (w/v) SDS, 0.09% (w/v) APS, and 0.33% (v/v) TEMED. Gels were used immediately or stored at 4 °C for up to 4 weeks. Protein samples were mixed with 4× SDS loading buffer containing dithiothreitol (DTT; Sigma-Aldrich) and heated at 90 °C for 5 min before loading. Electrophoresis was performed at a constant voltage of 120 V using 1× SDS running buffer (25 mM Tris-HCl pH 8.8, 192 mM glycine, 0.1% SDS). Proteins were visualized by staining with InstantBlue^{TM} Protein Stain (Abcam) for 1 h at room temperature with gentle agitation and imaged using a Fusion FX system (Vilber).

ATPase activity assay

The ATPase activity of β-DDM-solubilized TmrAB^{wt} was quantified using a Malachite Green-based colorimetric assay as described previously[44]. Detergent-solubilized TmrAB (0.6 µM) was incubated in ATPase buffer (20 mM HEPES-NaOH pH 7.5, 150 mM NaCl, 2 mM $MgCl_2$, 1 mM β-DDM) containing 3 mM ATP (Sigma-Aldrich) at 40 °C for 7 min. Autohydrolysis controls were prepared by incubation of ATP in ATPase buffer without protein. Reactions were quenched by adding 20 mM H_2SO_4, followed by incubation with 3 mM Malachite Green (Thermo Fisher Scientific), 0.2% (v/v) Tween20 (Carl Roth), and 1.5% (w/v) ammonium molybdate (Carl Roth) for 10 min at room temperature. The absorbance at 620 nm was recorded on a CLARIOstar v.5.20 R5 plate reader (BMG LABTECH).

Ensemble FRET measurements

The ATP binding and FRET characteristics of selected TmrAB variants were assessed by ensemble FRET. Labeled TmrAB (100 nM) was incubated with increasing concentrations of ATP at 42 °C for 5 min. Donor-excited emission was recorded from 550–700 nm with an excitation wavelength of 520 nm using a Clariostar v.5.20 R5 plate reader (BMG LABTECH). Acceptor emission intensities at 675 nm were plotted against ATP concentration and fitted with a hyperbolic function to determine the apparent dissociation constant ($K_{d,\ ATP}$) for each variant.

Functionalization of glass slides for single-molecule FRET analysis

Glass coverslips used for TmrAB immobilization in smFRET experiments were functionalized by PEGylation as described previously[45]. Coverslips (Carl Roth) were cleaned by sequential sonication in Milli-Q water and analytical-grade acetone (>99.9%; VWR International), followed by oxygen plasma treatment (0.3 mbar, 80% power, 15 min) using a Zepto plasma cleaner (Diener) and a 10 min incubation in methanol (Avantor, Gliwice, PL). Coverslips were then silanized by incubation for 30 min in a solution of 100 ml methanol, 5 ml acetic acid, and 3 ml 3-aminopropyltrimethoxysilane (APTES; Tokyo Chemical Industry). After silanization, sides were rinsed four times with methanol and dried under a nitrogen stream. Surface functionalization was achieved using a mixture of biotinylated-PEG (4 mol%) and nonbiotinylated-PEG (96 mol%; Rapp Polymer). The PEG solution was sandwiched between two coverslips and incubated overnight in a humidity chamber. Coverslips were then rinsed thoroughly with Milli-Q water and dried under nitrogen. To enhance passivation, a second PEGylation step was performed using 25 mM CH_3-PEG-NHS (333 Da; Thermo Fisher Scientific) under the same conditions. Finally, slides were rinsed with Milli-Q water, dried under nitrogen, and stored at –20 °C under argon until use.

Single-molecule FRET imaging

Single-molecule FRET (smFRET) experiments were performed using a flow chamber system (Ibidi). Chambers were assembled by placing a biotin-PEG-functionalized glass slide onto a µ-Slide I Luer Family flow channel (Ibidi), with the functionalized surface facing inward. All buffers and Milli-Q water were filtered through 0.2 µm filters (Sigma-Aldrich). Chambers were washed with 1 ml Milli-Q water and incubated with 0.2 mg ml^{-1} streptavidin (Sigma-Aldrich) at 4 °C for 30 min to allow binding to the biotin-PEG surface. Unbound streptavidin was removed by washing with 1 ml Milli-Q water. The surface was then treated with 0.3 mg ml^{-1} biotinylated-PEG_{11}-$Nb9F10^{S63C}$ at 4 °C for 45 min, followed flushing with 2 ml SEC buffer (20 mM HEPES-NaOH pH 7.5, 150 mM NaCl, 1 mM β-DDM). Detergent-solubilized, fluorophore-labeled TmrAB (100 nM) was added and incubated at 4 °C for 1 h. Unbound protein was removed by five washes with 1 ml TmrAB-SEC buffer. Chambers were equilibrated with 1 ml of imaging buffer containing 25 mM HEPES-NaOH (pH 7.5), 150 mM NaCl, 3 mM $MgCl_2$, 50 mM glucose, 5 mM Trolox, 7.5 U ml^{-1} pyranose oxidase, and 1 kU ml^{-1} catalase, supplemented with the desired ATP concentration. For EDTA trapping experiments, $MgCl_2$ was omitted and replaced with 3 mM ethylenediaminetetraacetic acid (EDTA; Sigma-Aldrich). smFRET data were acquired at 40 °C using alternating laser excitation (ALEX) on a total internal reflection fluorescence (TIRF) microscope (NanoImager S, ONI, Oxford, UK). Typically, 600 frames were recorded per region of interest (ROI) with 100 ms exposure time. Laser powers were 0.8 mW cm^{-2} (532 nm) and 0.9 mW cm^{-2} (640 nm). Data were recorded in 1-min intervals, except for $TmrAB^{NBD}$ variant in apo and 3 mM ATP conditions, where 3-min intervals were used to confirm that conformation transitions do not occur on timescales longer that one minute due to the reduced temperature.

Single-molecule FRET data analysis

Single-molecule FRET (smFRET) measurements were performed using alternating laser excitation (ALEX), allowing assignment of detected photons based on both excitation and emission wavelengths. Photon counts for each molecule were extracted using NanoImager software (ONI NanoImager, Development Build) and classified into three detection channels: donor excitation with donor emission ($f_{D_{ex}}^{D_{em}}$), donor excitation with acceptor emission ($f_{D_{ex}}^{A_{em}}$), and acceptor excitation with acceptor emission ($f_{A_{ex}}^{A_{em}}$). Traces were analyzed with DeepFRET[35] and manually curated. To minimize bias, a second researcher independently curated traces from both ATP-free and 3 mM ATP samples,

$$E = \frac{f_{D_{ex}}^{A_{em}}}{f_{D_{ex}}^{D_{em}} + f_{A_{ex}}^{A_{em}}} \quad (1)$$

$$S = \frac{f_{D_{ex}}^{D_{em}} + f_{D_{ex}}^{A_{em}}}{f_{D_{ex}}^{D_{em}} + f_{D_{ex}}^{A_{em}} + f_{A_{ex}}^{A_{em}}} \quad (2)$$

yielding 98% overlap between curations. FRET efficiency (*E*) and stoichiometry (*S*) were calculated as:

Population analysis was performed by constructing one-dimensional histograms of FRET efficiency (*E*) and stoichiometry (*S*) using OriginPro 2024 (OriginLab). Histograms were fitted with two Gaussian distributions corresponding to the ATP-free state (defined from apo samples) and the ATP-bound state (defined by a two-component fit at saturating ATP). Hidden Markov Modeling (HMM) of individual traces was performed using MASH-FRET[38] to distinguish dynamic from static molecules within each sample.

ATP-bound dwell times and distribution of conformational states

The ATP-bound dwell time (τ_d) was estimated as:

$$\tau_d = \tau_{\text{cycle}} \times f_{ATP-\text{bound}} \quad (3)$$

where $f_{\text{ATP-bound}}$ is the fraction of ATP-bound molecules derived from Gaussian fits of the FRET efficiency histograms (Fig. 3). This approach assumes (i) ATP hydrolysis occurs exclusively at the canonical NBS, with negligible contribution from the noncanonical site[9,11,14], and (ii) the majority of molecules are catalytically competent and continuously cycling.

The distribution of conformational states within ATP-bound FRET population (*E* = 0.86) of TmrAB^{PG} under turnover conditions (3 mM ATP) was determined using a two-state model:

$$E = f_{\text{open}} \times E_{\text{open}} + f_{\text{other}} \times E_{\text{other}} \quad (4)$$

where f_{open} is the fraction of OF$^{\text{open}}$ state (E_{open} = 0.63) readily resolved under trapping conditions (Fig. 4), and f_{other} represents the combined fraction of PG-closed states (OF$^{\text{occluded}}$/UR$^{\text{asym}}$/UR$^{\text{asym}}$*, E_{other} = 0.97).

Data availability

Source data are provided with this paper: DOI: *https://doi.org/10.25716/gude.0jbq-k1q6*.

Acknowledgements

This work was supported by the European Research Council (ERC Advanced Grant 101141396 to R.T.), the German Research Foundation via the Collaborative Research Center CRC 1507/P18 to R.T. and the Research Training Group (GRK 1986/B4.7 to R.T.). We thank Jan F.M. Stuke and Jonas Göhmann for their support in automating trace extraction from ONI NanoImager software, Dr. David Glück for guidance on lifetime measurements, and Tobias Nocker for preparing nanobodies used in the study. We are also grateful to the Wachtveitl lab (Goethe University Frankfurt) for access to their FluoTime 100 spectrometer (PicoQuant). Finally, we thank Dr. Rupert Abele, Dr. David Glück, Dr. Simon Trowitzsch, Inga Nold, and Andrea Pott for helpful comments on the manuscript and proofreading.

Additional information

Author contributions

M.P. prepared all TmrAB samples and carried out the experiments for this study. M.P. performed data analysis. Curated traces were independently checked by C.N. to avoid human bias. M.P. and C.N. prepared functionalized glass slides for single-molecule FRET. M.P. and R.T. wrote the manuscript. R.T. conceived and supervised the work.

Funding

Funder	Grant reference number	Author
EC | European Research Council (ERC)	https://doi.org/10.3030/101141396	Robert Tampé
Deutsche Forschungsgemeinschaft (DFG)	CRC 1507/P18	Robert Tampé
Deutsche Forschungsgemeinschaft (DFG)	GRK 1986/B4.7	Robert Tampé

Author ORCID iDs

Robert Tampé: https://orcid.org/0000-0002-0403-2160

References

1. **Davidson AL,** Dassa E, Orelle C, Chen J (2008) Structure, function, and evolution of bacterial ATP-binding cassette systems. *Microbiol Mol Biol Rev* **72**:317-364 https://doi.org/10.1128/mmbr.00031-07 | PubMed
2. **Rees DC,** Johnson E, Lewinson O (2009) ABC transporters: the power to change. *Nat Rev Mol Cell Biol* **10**:218-227 https://doi.org/10.1038/nrm2646 | PubMed
3. **Thomas C,** Tampé R (2020) Structural and mechanistic principles of ABC transporters. *Annu Rev Biochem* **89**:605-636 https://doi.org/10.1146/annurev-biochem-011520-105201 | PubMed
4. **Locher KP** (2016) Mechanistic diversity in ATP-binding cassette (ABC) transporters. *Nat Struct Mol Biol* **23**:487-493 https://doi.org/10.1038/nsmb.3216 | PubMed
5. **Thomas C,** et al. (2020) Structural and functional diversity calls for a new classification of ABC transporters. *FEBS Lett* **594**:3767-3775 https://doi.org/10.1002/1873-3468.13935 | PubMed
6. **Robey RW,** Pluchino KM, Hall MD, Fojo AT, Bates SE, Gottesman MM (2018) Revisiting the role of ABC transporters in multidrug-resistant cancer. *Nat Rev Cancer* **18**:452-464 https://doi.org/10.1038/s41568-018-0005-8 | PubMed
7. **Abele R,** Tampé R (2004) The ABCs of immunology: structure and function of TAP, the transporter associated with antigen processing. *Physiology (Bethesda)* **19**:216-224 https://doi.org/10.1152/physiol.00002.2004 | PubMed
8. **Kim J,** et al. (2015) Subnanometre-resolution electron cryomicroscopy structure of a heterodimeric ABC exporter. *Nature* **517**:396-400 https://doi.org/10.1038/nature13872 | PubMed
9. **Zutz A,** et al. (2011) Asymmetric ATP hydrolysis cycle of the heterodimeric multidrug ABC transport complex TmrAB from *Thermus thermophilus*. *J Biol Chem* **286**:7104-7115 https://doi.org/10.1074/jbc.m110.201178 | PubMed
10. **Nöll A,** et al. (2017) Crystal structure and mechanistic basis of a functional homolog of the antigen transporter TAP. *Proc Natl Acad Sci U S A* **114**:E438-E447 https://doi.org/10.1073/pnas.1620009114 | PubMed
11. **Hofmann S,** et al. (2019) Conformation space of a heterodimeric ABC exporter under turnover conditions. *Nature* **571**:580-583 https://doi.org/10.1038/s41586-019-1391-0 | PubMed
12. **Stefan E,** Hofmann S, Tampé R (2020) A single power stroke by ATP binding drives substrate translocation in a heterodimeric ABC transporter. *eLife* **9**:e55943 https://doi.org/10.7554/eLife.55943 | PubMed

13. **Stefan E,** et al. (2021) De novo macrocyclic peptides dissect energy coupling of a heterodimeric ABC transporter by multimode allosteric inhibition. *eLife* **10**:e67732 https://doi.org/10.7554/eLife.67732 | PubMed
14. **Barth K,** Rudolph M, Diederichs T, Prisner TF, Tampé R, Joseph B (2020) Thermodynamic basis for conformational coupling in an ATP-binding cassette exporter. *J Phys Chem Lett* **11**:7946-7953 https://doi.org/10.1021/acs.jpclett.0c01876 | PubMed
15. **Barth K,** Hank S, Spindler PE, Prisner TF, Tampé R, Joseph B (2018) Conformational coupling and trans-inhibition in the human antigen transporter ortholog TmrAB resolved with dipolar EPR spectroscopy. *J Am Chem Soc* **140**:4527-4533 https://doi.org/10.1021/jacs.7b12409 | PubMed
16. **Agam G,** et al. (2023) Reliability and accuracy of single-molecule FRET studies for characterization of structural dynamics and distances in proteins. *Nat Methods* **20**:523-535 https://doi.org/10.1038/s41592-023-01807-0 | PubMed
17. **Hellenkamp B,** et al. (2018) Precision and accuracy of single-molecule FRET measurements-a multi-laboratory benchmark study. *Nat Methods* **15**:669-676 https://doi.org/10.1038/s41592-018-0085-0 | PubMed
18. **Sasmal DK,** Pulido LE, Kasal S, Huang J (2016) Single-molecule fluorescence resonance energy transfer in molecular biology. *Nanoscale* **8**:19928-19944 https://doi.org/10.1039/c6nr06794h | PubMed
19. **Bartels K,** Lasitza-Male T, Hofmann H, Löw C (2021) Single-molecule FRET of membrane transport proteins. *ChemBioChem* **22**:2657-2671 https://doi.org/10.1002/cbic.202100106 | PubMed
20. **Lerner E,** et al. (2021) FRET-based dynamic structural biology: Challenges, perspectives and an appeal for open-science practices. *eLife* **10**:e60416 https://doi.org/10.7554/eLife.60416 | PubMed
21. **Nettels D,** Galvanetto N, Ivanović MT, Nüesch M, Yang T, Schuler B (2024) Single-molecule FRET for probing nanoscale biomolecular dynamics. *Nat Rev Phys* **6**:587-605 https://doi.org/10.1038/s42254-024-00748-7
22. **Wang L,** Johnson ZL, Wasserman MR, Levring J, Chen J, Liu S (2020) Characterization of the kinetic cycle of an ABC transporter by single-molecule and cryo-EM analyses. *eLife* **9**:e56451 https://doi.org/10.7554/eLife.56451 | PubMed
23. **Levring J,** Terry DS, Kilic Z, Fitzgerald G, Blanchard SC, Chen J (2023) CFTR function, pathology and pharmacology at single-molecule resolution. *Nature* **616**:606-614 https://doi.org/10.1038/s41586-023-05854-7 | PubMed
24. **Husada F,** et al. (2018) Conformational dynamics of the ABC transporter McjD seen by single-molecule FRET. *EMBO J* **37**:e100056 https://doi.org/10.15252/embj.2018100056 | PubMed
25. **Nocker C,** Pečak M, Nocker T, Fahim A, Sušac L, Tampé R. (2025) Single-molecule dynamics reveal ATP binding alone powers substrate translocation by an ABC transporter. *BioRxiv* 2025.2011.2027.690960 https://doi.org/10.1101/2025.11.27.690960
26. **Grossmann N,** Vakkasoglu AS, Hulpke S, Abele R, Gaudet R, Tampé R (2014) Mechanistic determinants of the directionality and energetics of active export by a heterodimeric ABC transporter. *Nat Commun* **5**:5419 https://doi.org/10.1038/ncomms6419 | PubMed
27. **Sun P,** et al. (2025) Substrate recognition diversity and transport dynamics of ABCC1. *Nat Commun* **16**:10499 https://doi.org/10.1038/s41467-025-65501-9 | PubMed
28. **Altman RB,** et al. (2011) Cyanine fluorophore derivatives with enhanced photostability. *Nat Methods* **9**:68-71 https://doi.org/10.1038/nmeth.1774 | PubMed
29. **Martin MI,** et al. (2023) Leveraging Baird aromaticity for advancement of bioimaging applications. *J Phys Org Chem* **36** https://doi.org/10.1002/poc.4449 | PubMed
30. **Kalinin S,** et al. (2012) A toolkit and benchmark study for FRET-restrained high-precision structural modeling. *Nat Methods* **9**:1218-1225 https://doi.org/10.1038/nmeth.2222 | PubMed
31. **Ha T,** Tinnefeld P (2012) Photophysics of fluorescent probes for single-molecule biophysics and super-resolution imaging. *Annu Rev Phys Chem* **63**:595-617 https://doi.org/10.1146/annurev-physchem-032210-103340 | PubMed

32. **Sindbert S,** et al. (2011) Accurate distance determination of nucleic acids via Förster resonance energy transfer: implications of dye linker length and rigidity. *J Am Chem Soc* **133**:2463-2480 https://doi.org/10.1021/ja105725e | PubMed

33. **Dale RE,** Eisinger J, Blumberg WE (1979) The orientational freedom of molecular probes. The orientation factor in intramolecular energy transfer. *Biophys J* **26**:161-193 https://doi.org/10.1016/s0006-3495(79)85243-1 | PubMed

34. **van der Meer BW** (2002) Kappa-squared: from nuisance to new sense. *J Biotechnol* **82**:181-196 https://doi.org/10.1016/s1389-0352(01)00037-x | PubMed

35. **Thomsen J,** et al. (2020) DeepFRET, a software for rapid and automated single-molecule FRET data classification using deep learning. *eLife* **9**:e60404 https://doi.org/10.7554/eLife.60404 | PubMed

36. **Hohlbein J,** Craggs TD, Cordes T (2014) Alternating-laser excitation: single-molecule FRET and beyond. *Chem Soc Rev* **43**:1156-1171 https://doi.org/10.1039/c3cs60233h | PubMed

37. **Asher WB,** et al. (2021) Single-molecule FRET imaging of GPCR dimers in living cells. *Nat Methods* **18**:397-405 https://doi.org/10.1038/s41592-021-01081-y | PubMed

38. **Hadzic M,** Borner R, Konig SLB, Kowerko D, Sigel RKO (2018) Reliable state identification and state transition detection in fluorescence intensity-based single-molecule Förster Resonance Energy-Transfer data. *J Phys Chem B* **122**:6134-6147 https://doi.org/10.1021/acs.jpcb.7b12483 | PubMed

39. **Dimura M,** Peulen TO, Hanke CA, Prakash A, Gohlke H, Seidel CA (2016) Quantitative FRET studies and integrative modeling unravel the structure and dynamics of biomolecular systems. *Curr Opin Struct Biol* **40**:163-185 https://doi.org/10.1016/j.sbi.2016.11.012 | PubMed

40. **Lam K,** Tajkhorshid E (2020) Membrane interactions of Cy3 and Cy5 fluorophores and their effects on membrane-protein dynamics. *Biophys J* **119**:24-34 https://doi.org/10.1016/j.bpj.2020.05.027 | PubMed

41. **Grabenhorst L,** Sturzenegger F, Hasler M, Schuler B, Tinnefeld P (2024) Single-molecule FRET at 10 MHz count rates. *J Am Chem Soc* **146**:3539-3544 https://doi.org/10.1021/jacs.3c13757 | PubMed

42. **Bonhomme L,** et al. (2025) Triple labeling resolves a GPCR intermediate state by using three-color single molecule FRET. *J Am Chem Soc* **147**:17689-17700 https://doi.org/10.1021/jacs.4c18364 | PubMed

43. **Yim SW,** et al. (2012) Four-color alternating-laser excitation single-molecule fluorescence spectroscopy for next-generation biodetection assays. *Clin Chem* **58**:707-716 https://doi.org/10.1373/clinchem.2011.176958 | PubMed

44. **Diederichs T,** Tampé R (2021) Single cell-like systems reveal active unidirectional and light-controlled transport by nanomachineries. *ACS Nano* **15**:6747-6755 https://doi.org/10.1021/acsnano.0c10139 | PubMed

45. **Chandradoss SD,** Haagsma AC, Lee YK, Hwang JH, Nam JM, Joo C (2014) Surface passivation for single-molecule protein studies. *J Vis Exp* **50549** https://doi.org/10.3791/50549 | PubMed

46. **Chaptal V,** et al. (2022) Substrate-bound and substrate-free outward-facing structures of a multidrug ABC exporter. *Sci Adv* **8**:eabg9215 https://doi.org/10.1126/sciadv.abg9215 | PubMed

Peer reviews

Reviewer #1 (Public review):

Summary:

Pecak et al have deciphered the conformational dynamics of a heterodimeric model ABC transporter, TmrAB, a functional homolog of the human antigen transporter TAP, using single-molecule Forster resonance energy and fluorophores attached to residues at either nucleotide binding domains or periplasmic gate. The analysis not only differentiated ATP-free and bound states but also enabled the real-time monitoring of protein conformational

changes, precisely dissecting transport cycles and resolving transient intermediates. This study is absolutely significant in providing and establishing a general pipeline delineating the conformational dynamics in heterodimeric ABC transporters.

Strengths:

The scientific study is very well documented for experimental design, results, and conclusions supported by the experimental data. The authors have determined the conformational dynamics of TmrAB across different ATP concentrations, including physiological ones, and resolved an outward open state and other conformational states consistent with previous cryoEM and DEER studies.

Weaknesses:

The scientific study needs a bit of in-depth analysis with respect to consistency in Kd and its implications on the mechanism.

https://doi.org/10.7554/eLife.110967.1.sa1

Reviewer #2 (Public review):

In their manuscript entitled 'ATP-driven conformational dynamics reveal hidden intermediates in a heterodimeric ABC transporter', Pečak et al. use elegant single-molecule FRET experiments in detergent to investigate the heterodimeric ABC transporter TmrAB. By combining simulations of the transporter's accessible volume with elegant trapping strategies, the authors identify an unresolved outward-facing open state and conclude that it is usually obscured by a rapidly interconverting ATP-bound ensemble. Overall, the study demonstrates that smFRET can resolve the short-lived intermediate states of TmrAB and potentially other ABC transporters that are obscured in ensemble measurements.

It is a very interesting study that highlights the power of combining high-resolution structural information with spectroscopic approaches. I have three major points and a few minor criticisms.

Major points:

(1) The main weakness is that the authors base their conclusions on a very limited set of FRET pairs. While TmrAB has been extensively studied in terms of its structure, the authors should at least acknowledge this limitation more clearly.

(2) Most smFRET distributions were fitted with one, two, or three Gaussians. However, in several cases, additional populations with noticeable amplitudes appear to be present (e.g., Figure 3c at 0.1 mM and 3 mM ATP; Figure 4a, apo; Figure 4c, 0.3 mM R9L). Could the authors clarify why these populations were not included in the analysis?

(3) Figure 3c (3 mM ATP): Is it truly possible to distinguish the two states in this distribution?

https://doi.org/10.7554/eLife.110967.1.sa0

Author response:

> ***Public Reviews:***
>
> ***Reviewer #1 (Public review):***
>
> *Summary:*

> *Pecak et al have deciphered the conformational dynamics of a heterodimeric model ABC transporter, TmrAB, a functional homolog of the human antigen transporter TAP, using single-molecule Forster resonance energy and fluorophores attached to residues at either nucleotide binding domains or periplasmic gate. The analysis not only differentiated ATP-free and bound states but also enabled the real-time monitoring of protein conformational changes, precisely dissecting transport cycles and resolving transient intermediates. This study is absolutely significant in providing and establishing a general pipeline delineating the conformational dynamics in heterodimeric ABC transporters.*

We thank the reviewer for this accurate and thoughtful summary of our work and its broader significance. We agree that the combination of single-molecule FRET with orthogonal validation approaches enables mechanistic resolution of conformational states and transitions that are not accessible by ensemble measurements. In particular, this framework allows direct discrimination of ATP-free and ATP-bound conformations, real-time tracking of transport cycle progression, and identification of transient intermediates in the heterodimeric ABC transporter TmrAB. We further agree that these capabilities support a generalizable strategy for dissecting conformation dynamics in related ABC transporters.

> *Strengths:*
>
> *The scientific study is very well documented for experimental design, results, and conclusions supported by the experimental data. The authors have determined the conformational dynamics of TmrAB across different ATP concentrations, including physiological ones, and resolved an outward open state and other conformational states consistent with previous cryoEM and DEER studies.*
>
> *Weaknesses:*
>
> *The scientific study needs a bit of in-depth analysis with respect to consistency in K_d and its implications on the mechanism.*

The apparent $K_{d,ATP}$ values were determined using two complementary approaches that report on different aspects of the system. Ensemble FRET measurements yielded values of 51° ± 38° μM ($TmrAB^{NBD}$), 68° ± 25° μM ($TmrAB^{PG}$), and 95° ± 26° μM ($TmrAB^{PG\_EQ}$), which are in good agreement with previously reported biochemical estimates (~100° μM for $TmrAB^{EQ}$) (Stefan et al, 2020). The slightly elevated value observed for the E→Q variant may reflect modest perturbation of nucleotide handling in this slow-turnover background. Notably, the close agreement between labeled and unlabeled variants indicates that fluorophore attachment does not measurably affect ATP binding.

In contrast, smFRET-derived $K_{d,ATP}$ values (13° ± 1° μM for $TmrAB^{NBD}$ and 2° ± 1° μM for $TmrAB^{PG}$) are systematically lower. This difference likely arises from the difficulty of deconvoluting overlapping FRET populations at sub-$K_{d,ATP}$ concentrations, particularly for $TmrAB^{PG}$, where state assignment is less well separated. Despite this quantitative offset, both approaches consistently indicate ATP saturation well below physiological concentrations and therefore support the same mechanistic conclusion that ATP binding drives conformational switching in TmrAB.

> ***Reviewer #2 (Public review):***
>
> *In their manuscript entitled 'ATP-driven conformational dynamics reveal hidden intermediates in a heterodimeric ABC transporter', Pečak et al. use elegant single-molecule FRET experiments in detergent to investigate the heterodimeric ABC transporter TmrAB. By combining simulations of the transporter's accessible volume with elegant trapping strategies, the authors identify an unresolved outward-facing open state and*

> *conclude that it is usually obscured by a rapidly interconverting ATP-bound ensemble. Overall, the study demonstrates that smFRET can resolve the short-lived intermediate states of TmrAB and potentially other ABC transporters that are obscured in ensemble measurements.*
>
> *It is a very interesting study that highlights the power of combining high-resolution structural information with spectroscopic approaches. I have three major points and a few minor criticisms.*

We thank the reviewer for the thoughtful and constructive evaluation of our manuscript and for highlighting the strength of combining structural and single-molecule approaches. We have addressed all major and minor points in detail below and revised the manuscript where appropriate to clarify limitations, justify analysis choices, and improve transparency.

> *Major points:*
>
> *(1) The main weakness is that the authors base their conclusions on a very limited set of FRET pairs. While TmrAB has been extensively studied in terms of its structure, the authors should at least acknowledge this limitation more clearly.*

We agree that our conclusions are based on a limited number of FRET reporter pairs, and we now explicitly state this limitation in the revised manuscript. The chosen labeling positions were selected to probe two functionally critical regions—the nucleotide-binding domains and the periplasmic gate—based on prior structural and spectroscopic evidence. While this represents sparse sampling of the full conformational space, it is consistent with typical smFRET studies of membrane transporters, where experimental constraints generally limit the number of simultaneously accessible labeling positions (Asher et al, 2021; Asher et al, 2022; Levring et al, 2023; Wang et al, 2020).

Importantly, both independent reporter variants yield consistent ATP-dependent population shifts, supporting the robustness of the observed trends. We further clarify that additional labeling sites could, in principle, resolve finer structural sub-states; however, given the already limited population separation in the current variants, such extensions would likely provide diminishing returns in state resolvability under the present experimental conditions. This trade-off is now explicitly discussed.

> *(2) Most smFRET distributions were fitted with one, two, or three Gaussians. However, in several cases, additional populations with noticeable amplitudes appear to be present (e.g., Figure 3c at 0.1 mM and 3 mM ATP; Figure 4a, apo; Figure 4c, 0.3 mM R9L). Could the authors clarify why these populations were not included in the analysis?*

We thank the reviewer for this careful observation. Low-amplitude subpopulations are occasionally detected in individual histograms; however, they were not included in the quantitative model because they do not meet criteria for reproducibility, amplitude robustness, or structural assignability. Specifically, these features vary between replicates, contribute minimally to total population, and cannot be mapped to structurally or biochemically defined states based on available cryo-EM (Hofmann et al, 2019), DEER/PELDOR (Barth et al, 2018; Barth et al, 2020), or accessible-volume simulations.

Similar minor subpopulations have been reported in smFRET studies and often attributed to photophysical or labeling heterogeneity effects (Asher et al, 2022; Husada et al, 2018). To avoid over-parameterization, we therefore restricted analysis to reproducible, structurally supported states. This rationale is now clarified in the revised manuscript.

> *(3) Figure 3c (3 mM ATP): Is it truly possible to distinguish the two states in this distribution?*

We agree that state separation in the TmrAB^{PG} variant is limited (ΔE° = °0.11), and we now explicitly acknowledge this constraint in the manuscript. To improve robustness under these conditions, we used a constrained fitting strategy in which the apo-state distribution was fixed from nucleotide-free measurement, reducing parameter degeneracy during fitting of ATP-bound datasets.

While single-molecule trajectory-based approaches such as Hidden Markov Modeling would be ideal for resolving dynamic interconversion, this was not feasible due to the low fraction of dynamic traces at the available temporal resolution. We therefore rely on population-level analysis, which remains consistent across replicates and reporter variants.

Notably, independent measurements from two reporter positions (TmrAB^{NBD} and TmrAB^{PG}) yield similar ATP-bound population fractions at saturating ATP concentrations (~77% vs. ~80%), supporting the robustness of the inferred state distribution despite partial overlap.

References

Asher WB, Geggier P, Holsey MD, Gilmore GT, Pati AK, Meszaros J, Terry DS, Mathiasen S, Kaliszewski MJ, McCauley MD, Govindaraju A, Zhou Z, Harikumar KG, Jaqaman K, Miller LJ, Smith AW, Blanchard SC, Javitch JA (2021) Single-molecule FRET imaging of GPCR dimers in living cells. Nat Methods 18: 397–405. doi:10.1038/s41592-021-01081-y

Asher WB, Terry DS, Gregorio GGA, Kahsai AW, Borgia A, Xie B, Modak A, Zhu Y, Jang W, Govindaraju A, Huang LY, Inoue A, Lambert NA, Gurevich VV, Shi L, Lefkowitz RJ, Blanchard SC, Javitch JA (2022) GPCR-mediated beta-arrestin activation deconvoluted with single-molecule precision. Cell 185: 1661–1675 e1616. doi:10.1016/j.cell.2022.03.042

Barth K, Hank S, Spindler PE, Prisner TF, Tampé R, Joseph B (2018) Conformational coupling and trans-inhibition in the human antigen transporter ortholog TmrAB resolved with dipolar EPR spectroscopy. J Am Chem Soc 140: 4527–4533. doi:10.1021/jacs.7b12409

Barth K, Rudolph M, Diederichs T, Prisner TF, Tampé R, Joseph B (2020) Thermodynamic basis for conformational coupling in an ATP-binding cassette exporter. J Phys Chem Lett 11: 7946–7953. doi:10.1021/acs.jpclett.0c01876

Hofmann S, Januliene D, Mehdipour AR, Thomas C, Stefan E, Brüchert S, Kuhn BT, Geertsma ER, Hummer G, Tampé R, Moeller A (2019) Conformation space of a heterodimeric ABC exporter under turnover conditions. Nature 571: 580–583. doi:10.1038/s41586-019-1391-0

Husada F, Bountra K, Tassis K, de Boer M, Romano M, Rebuffat S, Beis K, Cordes T (2018) Conformational dynamics of the ABC transporter McjD seen by single-molecule FRET. EMBO J 37: e100056. doi:10.15252/embj.2018100056

Levring J, Terry DS, Kilic Z, Fitzgerald G, Blanchard SC, Chen J (2023) CFTR function, pathology and pharmacology at single-molecule resolution. Nature 616: 606–614. doi:10.1038/s41586-023-05854-7

Nocker C, Pečak M, Nocker T, Fahim A, Sušac L, Tampé R (2026) Single-molecule dynamics reveal ATP binding alone powers substrate translocation by an ABC transporter. Nat Commun 17 doi:10.1038/s41467-026-70021-1

Nöll A, Thomas C, Herbring V, Zollmann T, Barth K, Mehdipour AR, Tomasiak TM, Bruchert S, Joseph B, Abele R, Olieric V, Wang M, Diederichs K, Hummer G, Stroud RM, Pos KM, Tampé R (2017) Crystal structure and mechanistic basis of a functional homolog of the antigen transporter TAP. Proc Natl Acad Sci U S A 114: E438–E447. doi:10.1073/pnas.1620009114

Stefan E, Hofmann S, Tampé R (2020) A single power stroke by ATP binding drives substrate translocation in a heterodimeric ABC transporter. eLife 9: e55943. doi:10.7554/eLife.55943

Wang L, Johnson ZL, Wasserman MR, Levring J, Chen J, Liu S (2020) Characterization of the kinetic cycle of an ABC transporter by single-molecule and cryo-EM analyses. eLife 9: e56451. doi:10.7554/eLife.56451

https://doi.org/10.7554/eLife.110967.1.sa3